Linking microbial community composition, microbial biomass and extracellular polymeric substances to organic matter lability gradients in sediments of the tidal Elbe River

Gebert, Julia; Böhnke-Brandt, Stefanie; Zander, Florian; Indenbirken, Daniela; Bergmann, Lutgardis; Krohn, Ines; Perner, Mirjam

DOI
10.1016/j.scitotenv.2025.180614

Publication date
2025

Document Version
Final published version

Published in
Science of the Total Environment

Science of the Total Environment 1002 (2025) 180614

Contents lists available at ScienceDirect

Science of the Total Environment

journal homepage: www.elsevier.com/locate/scitotenv

Linking microbial community composition, microbial biomass and extracellular polymeric substances to organic matter lability gradients in sediments of the tidal Elbe River

Julia Gebert [a,b,1], Stefanie Böhnke-Brandt [c,*,1], Florian Zander [a], Daniela Indenbirken [d], Lutgardis Bergmann [e], Ines Krohn [e], Mirjam Perner [c]

[a] Delft University of Technology, Faculty of CITG, Department of Geoscience & Engineering, Stevinweg 1, 2628 CN, Delft, the Netherlands
[b] Technische Universität Braunschweig, Leichtweiß-Institute for Hydraulic Engineering and Water Resources, Beethovenstr. 51a, 38106, Braunschweig, Germany
[c] GEOMAR Helmholtz Centre for Ocean Research Kiel, Department of Marine Biogeochemistry, Research Group Geomicrobiology, Wischhofstr. 1-3, 24148, Kiel, Germany
[d] Leibniz Institute for Virology, Martinistr. 52, 20251, Hamburg, Germany
[e] University of Hamburg, Faculty of Mathematics, Informatics and Natural Sciences, Department of Biology, Institute of Plant Science and Microbiology, Microbiology and Biotechnology, Ohnhorststr. 18, 22609, Hamburg, Germany

HIGHLIGHTS

- Organic matter availability is key driver shaping microbial community composition.
- More labile carbon reduces bacterial but fosters archaeal diversity and vice versa.
- Archaea dominate terminal carbon release in spite of low relative abundances (<1 %).
- Microbial taxon richness to biomass ratio is an indicator for carbon lability.
- EPS composition reflects carbon lability and metabolic activity gradients.

GRAPHICAL ABSTRACT

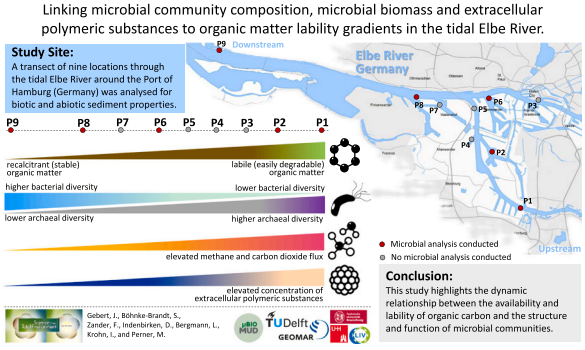

ARTICLE INFO

Keywords:
Sediments
Carbon fluxes
Microbial community
Syntrophy

ABSTRACT

The port of Hamburg represents a transition zone between upstream, shallow regions of high net primary production and downstream deep and more turbulent waters in the tidal Elbe River in northwestern Germany. Correspondingly, strong gradients of degradable organic matter (OM) on a distance of a few river kilometers had been identified. This study links microbial community composition using 16S metagenomic amplicons and extracellular polymeric substances (EPS) composition to the observed gradients of sediment OM lability. It was hypothesized that lability gradients caused by higher concentrations of biogenic, autochthonous OM upstream and greater share of already stabilized OM downstream reflect in gradients of microbial community composition, diversity and EPS characteristics.

* Corresponding author.
E-mail address: sboehnke-brandt@geomar.de (S. Böhnke-Brandt).
[1] First authors.

https://doi.org/10.1016/j.scitotenv.2025.180614
Received 17 June 2025; Received in revised form 18 September 2025; Accepted 23 September 2025
Available online 3 October 2025

Indeed, available OM was found to act as key driver regulating syntrophic microbial community composition and associated metabolic features, with location-specific overriding the effect of seasonal variations. Upstream sites with high available OM featuring lower bacterial but increased archaeal diversity and elevated methane and carbon dioxide fluxes, whereas lower OM lability downstream fostered a more diverse bacterial but decreased archaeal diversity. The ratio between microbial taxon richness and biomass correlated inversely with OM transformation rates. These patterns also reflected in increased EPS concentration produced in response to metabolic needs (i.e. polysaccharides and proteins), whereas structural components such as lipids, which can be more resistant under the prevailing anoxic conditions, remained more evenly distributed along the transect. Although bacterial relative abundances exceeded archaeal abundances (<1 %) by far, archaeal functional significance remained pivotal for the final release of carbon as methane and carbon dioxide under the mostly reducing conditions in the deposited sediment.

1. Introduction

The tidal Elbe River around the port of Hamburg is characterized by strong upstream-downstream spatial gradients of net primary production. The input of easily degradable organic matter (OM) of planktonic origin fuels carbon-driven ecosystem transitions and is identified as a hotspot of microbial metabolism (Norbisrath et al., 2022). After die-off, flocculation and sedimentation, suspended biogenic OM associates with the mineral phase of the near-riverbed sediments during decay and transformation. The deposited sediments also contain OM of, for example, terrestrial origin from eroded topsoils in the catchment or from anthropogenic sources, such as surface runoff or sewage treatment effluent. Corresponding to the source gradient of biogenic OM, the sediments show higher concentrations of total organic carbon and a higher degradability of sediment OM upstream Zander et al. (2022). Inversely, the share of carbon present in organo-mineral associations is higher downstream Zander et al. (2022), which are postulated to shield OM from microbial degradation (Keil and Mayer, 2014). These gradients result in different boundary conditions for the microbial community with respect to available carbon. Mostly, the sediments along the investigated transect rest under anoxic conditions, as evidenced by negative redox potentials (Gebert and Zander, 2024) where microbially mediated oxidation of sulphides, nitrification and carbon mineralization are the largest contributors to the oxygen consumption potential (Spieckermann et al., 2022). Especially the low-flow areas (such as closed-off harbour basins), in which the hydrodynamic conditions allow for sedimentation of fine-grained OM, function as a source of methane (CH_4) (Zander et al., 2023). Interactions between microorganisms and OM quality along ecosystem transitions have not yet been adequately quantified or incorporated into aquatic carbon budgets.

Further to the role of OM decay in freshwaters for continental greenhouse gas fluxes, OM also affects the physical behaviour of sediments in the water. OM connects mineral particles and thus affects floc formation (Deng et al., 2019), settlement, consolidation and the resulting strength of the sediment (Jommi et al., 2019) and flow behaviour (Shakeel et al., 2022; Zander et al., 2022). Wurpts and Torn (2005) proposed that microbially formed extracellular polymeric substances (EPS) decrease yield point and viscosity of saline fluidized sediments. EPS have also been shown to profoundly influence bedform dynamics, increasing the time for development of bedforms for already small quantities of EPS (Malarkey et al., 2015).

This study links microbial community composition and EPS concentration and composition to gradients of OM lability in sediments of the tidal Elbe River. It was hypothesized that lability gradients caused by higher concentrations of biogenic, autochthonous OM upstream and greater share of already stabilized (recalcitrant) OM downstream reflect gradients of microbial community composition, diversity and the presence and composition of extracellular polymeric substances.

2. Study area and sampling approach

The investigation area is located around the port of Hamburg in the tidal Elbe River. Using the concentration of zinc (Zn) in the particle size fraction of <20 μm as tracer (Groengroeft et al., 1998) shows that sediments upstream of approximately river km 619–620 originate from the upstream catchment area. Sediment that is deposited further downstream is primarily of North Sea origin (Reese et al., 2019; Zander et al., 2023), imported through the asymmetry of flood and ebb tide velocity distribution (Schoer, 1990), also referred to as tidal pumping. Nine locations within the tidal Elbe River around the Port of Hamburg (Fig. 1 in Gebert and Zander, 2024; see also Fig. 1) were sampled on average every two months in 2018. These locations present sedimentation hotspots with increased deposition rates of fine-grained sediments, requiring enhanced maintenance activity by the port to provide the required navigable depths. Of these nine locations, five were identified as priority locations regarding port maintenance and selected for more detailed investigations, including the study of the microbial community. At each location, between three and five sediment cores per sampling event were retrieved using a core sampler. For each core, up to four (if present) different layers were distinguished from top to bottom: suspended particulate matter (SPM), fluid mud (FM), pre-consolidated sediment (PS), and consolidated sediment (CS). These layers were separated and a mixed sample per layer prepared from the respective material of the multiple cores. From these, aliquots were frozen on board at −18 °C immediately after sampling for microbial community analyses while a further aliquot was stored cool for extraction of EPS. Further, aliquots of these mixed samples were used for the analysis of the sediment's biogeochemical properties, including the decay of OM. Microbial community composition was analysed on samples from locations P1, P2, P6, P8 and P9.

Along the transect, bacterial groups dominated the benthic microbial communities across all sites and seasons, while relative abundance of micro algae peaked in June (up to 25 %) (Fig. 1, Supplementary Figs. S1 and S2). Archaeal relative abundance remained consistently below 1 % in all samples. In this study, we provide more detailed insights into the microbial community composition and analyse correlations with sediment characteristics along the organic matter lability gradient found in River Elbe sediments.

3. Materials and methods

3.1. Standard properties of pore water and solids

The analysis of standard solids properties included total nitrogen (TN; ISO 16168:2012), total organic carbon (TOC; ISO10694:1995), water content (WC, ISO 11465:1993), redox potential (Eh; ISO 38404:2012), particle size distribution (ISO11277:2009), pH-value (pH; ISO 15933:2012), electrical conductivity (EC; ISO 27888:1993), in the filtrated pore water ammonium (NH_4^+; ISO 11732:2005) and silicic acid (as SiO_2; 38405-21:1990). OM fractions were analysed with an acid-base fractionation method that uses the aggregation/precipitation and dissolution properties of natural OM established by the International Humic Substances Society (IHSS) to determine acid-base-extractable DOM humic acid (HA), fulvic acid (FA), hydrophobic neutrals (HoN)

and hydrophilic acids (Hi) as described in Van Zomeren and Comans (2007), Straathof et al. (2014) and Zander et al. (2023).

3.2. Anaerobic and aerobic carbon degradability

Long-term (>500 days) release of CO_2-C and CH_4-C under aerobic and anaerobic conditions was analysed under standardized conditions in the laboratory. For quantification of degradability under anaerobic conditions, approximately 200 g of freshly sampled sediment were placed into 500 mL glass bottles in triplicate, sealed with a butyl rubber stopper and secured with a screw cap. The bottle headspace was flushed with N_2 to establish anaerobic conditions and bottles were incubated at 36 °C in the dark. Anaerobic carbon release was calculated from the increase in headspace pressure in combination with gas chromatographic (Da Vinci Laboratory Solutions) analyses of headspace composition. OM degradability under oxic conditions was quantified by placing around 15 g of sediment in 1000 mL glass bottles sealed with a butyl rubber stopper and incubated at 20 °C in the dark. Carbon was calculated from the increase in headspace CO_2 concentration over time. To avoid inhibition of respiratory activity by high CO_2 concentrations, the bottle headspace was flushed with air when concentrations exceeded 3 vol%. In all cases, the share of CO_2-C dissolved in the aqueous phase was calculated using the CO_2 concentration and the pressure in the bottle headspace and the temperature-corrected solubility of CO_2 in water as given by Henry's constant (given in Sander, 2015). Possible changes in sample moisture content (not detected) were monitored by weighing the bottles. Under anoxic conditions OM decay rates are lower. Since the purpose of the studies by Zander et al. (2023, 2022) was to exhaust OM decay as much as possible in order to extrapolate the degradable share with high certainty, a higher incubation temperature was chosen than for the oxic incubations. In order to compare anoxic and oxic C release, data from the anoxic incubations were normalized to a temperature of 20 °C based on the known temperature dependency of both processes, as researched on sediment samples from this study (Zander, 2022).

3.3. Composition of the microbial community

3.3.1. DNA extraction and 16S amplicon library preparation

To study the composition of the prokaryotic community, 16S rRNA gene amplicon libraries compatible with the Illumina MiSeq System were prepared. Metagenomic DNA was first extracted from around 300 mg sample using the NucleoSpin DNA Soil Mini kit (7.4 and 186 ng μl^{-1} with a 260/280 nm ratio ranging from 1.76 to 1.87) according to the specifications of the manufacturer (Macherey-Nagel, Düren, Germany). The metagenomic DNA was then used as a template (12.5 ng) for the amplification of (i) the 16S bacterial hypervariable V3/V4 regions using the primer pair S-D-Bac-0341-b-S-17 and S-D-Bac-0785-a-A-21 (Klindworth et al., 2013) and (ii) the 16S archaeal hypervariable V4/V5 regions using the two primer pairs Arch 519F / Arch 915R, (Ding et al., 2017) and Arch 524F / Arch 958R (Cerqueira et al., 2017), respectively. Duplicate PCR reactions were performed for each of the three primer sets (total of 3 × 2 PCRs per sample) using Kapa Hifi HotStart Ready Mix (Kapa Biosystems, Boston, MA, USA) according to the instructions in the manufacturer's protocol. PCR conditions were set as follows: 3 min initial denaturation followed by 25 cycles of denaturation at 95 °C for 30 s, annealing at 55 °C and 63 °C for amplification of the bacterial and the archaeal 16S rRNA gene, respectively, and extension at 72 °C for 30

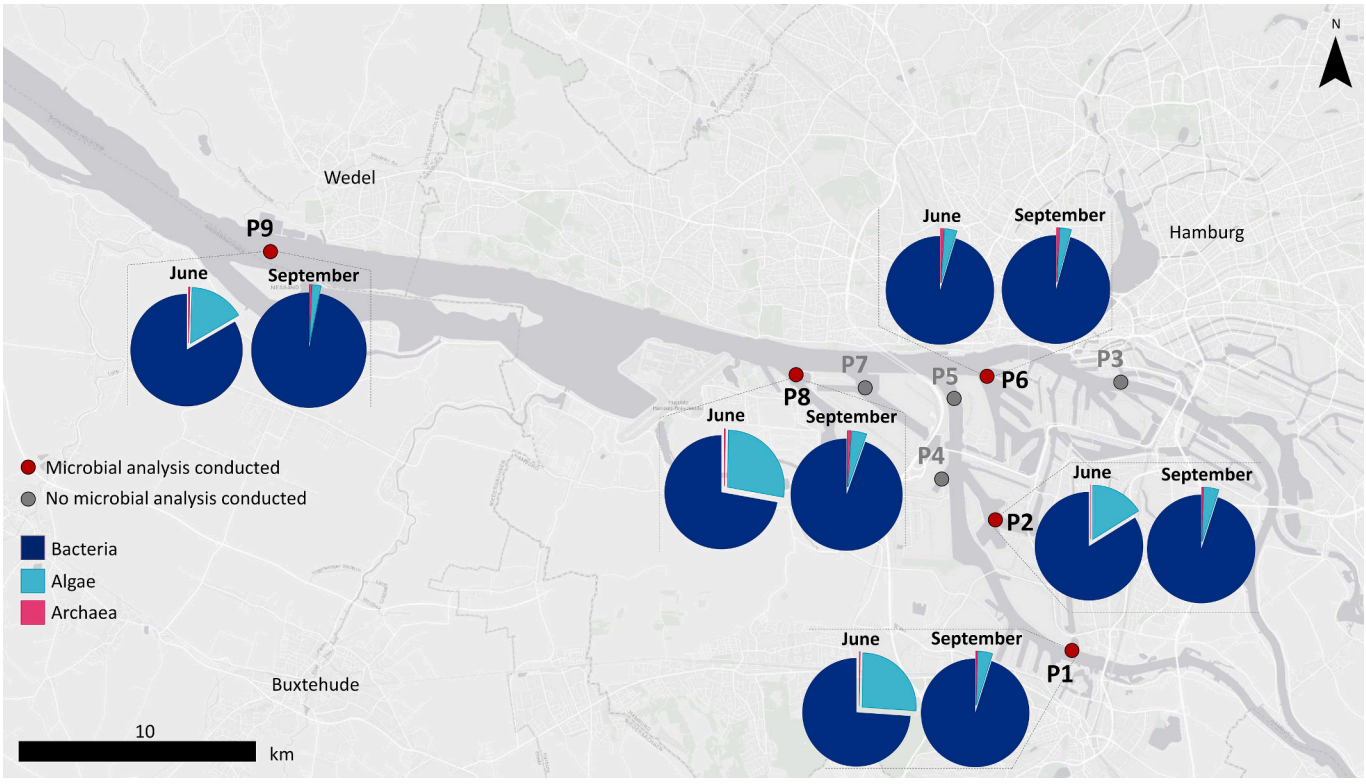

Fig. 1. Study area around the Port of Hamburg with sampling locations between river km 616 (P1, upstream) and 643 (P9, downstream). Sampling sites where microbial analysis were carried out are marked with black dots, while sites where only chemical analysis were performed are shown with dark grey dots. Abundance of 16S rRNA transcripts of bacteria, archaea and algae determined via quantitative PCR (qPCR) along the investigated Elbe River transect are shown as a pie chart next to the respective sampling site. qPCR data are presented as a percentage of the total RNA transcripts relative to bacterial 16S rRNA transcript. Data from June and September for the PS layer were chosen as a representative sample. Additional qPCR data for the months of August and November and for other sediment layers, are shown in Figs. S1 and S2. The map of the Elbe River was created with ArcMap™ Desktop 10.8.1 (®Esri, HERE, Garmin, ©OpenStreetMap contribution, and the GIS user community).

s. After the pooled bacterial (1 × 2) and archaeal (2 × 2) 16S rRNA gene amplifications were purified using the Agencourt AMPure XP Reagent (Beckman Coulter, Brea, CA, USA) multiplexing indices and Illumina® sequencing adapters were added by using the Nextera® XT Index Kit (Illumina) and the Kapa Hifi HotStart Ready Mix (Kapa Biosystems) under the same PCR conditions mentioned above, but with 8 cycles. The quality of bead-based purified (AMPure XP), indexed samples was then verified on the 2100 Bioanalyzer (Agilent Technologies, using the DNA High Sensitivity Chip). The 16S rRNA metagenomic library was sequenced by paired-end sequencing in a 2 × 300 bp run on the Illumina MiSeq platform (Illumina, St. Diego, USA) at the Leibniz Institute for Virology, Hamburg, Germany.

3.3.2. QIME, R, visualization

Sequences were processed using the Qiime2 environment (Bolyen et al., 2019). The filtering and merging of demultiplexed raw reads were performed using the dada2-plugin with default settings and removal of the primer sequences (Callahan et al., 2016). For taxonomic assignments the SILVA database release 138 (Quast et al., 2013) was pre-trained with the respective primer pairs for bacteria and archaea (Kaehler et al., 2019). The assignments were computed using the feature-classifier plugin (classify sklearn) with default settings and the pre-trained SILVA classifier (Kaehler et al., 2019). The phylogeny was calculated using the "align-to-tree-mafft-fasttree" pipeline (Price et al., 2010). Visualization and further statistical analysis were performed in R: A language and environment for statistical computing. R Foundation for Statistical Computing, Vienna, Austria. URL https://www.R-project.org/ using the microeco package (Liu et al., 2021). Principle Coordinate Analysis (PCoA) were performed based on weighted and unweighted UniFrac distances to calculate beta diversity between the different sampling locations, time points, and layers with rarefaction set to a sampling depth 7000 for bacteria and 3800 for archaea. Differential abundance analysis (DAA) were performed using the Random Forest (rf) method, with no *p*-value adjustment and rarefaction set as 2000 for bacteria and 4000 for archaea, respectively. Feature importance was determined based on the MeanDecreaseGini, indicating the importance of each taxon in the Random Forest classification. Taxa with higher Mean Decrease Gini values are considered more important for distinguishing between groups.

3.3.3. Real time quantitative PCR (qPCR)

The relative abundances of bacteria, archaea and microalgae were determined via real-time quantitative PCR (qPCR). Therefore, a total of 20 ng of isolated metagenomic DNA was used as a template for amplifying the hypervariable V3/V4 regions of the bacterial 16S rRNA gene, the hypervariable V4/V5 regions of archaeal 16S rRNA gene and the hypervariable V8/V9 region of the algal 18S rRNA region. For bacteria and archaea, the same primer pairs that have been used for Illumina® sequencing were used, but for qPCR the Illumina® adaptor overhang nucleotide sequence was removed. For Microalgae the primer pair V8f-1422-18S (Bradley et al., 2016) / 1510r//IlluO (Amaral-Zettler et al., 2009) was used. The SYBR® Select Master Mix, CFX (Applied Biosystems® by Life TechnologiesTM) was utilized to set up the qPCR reaction. The amplification was performed with the CFX96TM Real-Time System C1000 Touch Thermal Cycler (BioRad, Hercules, CA, USA) under the following conditions: 95 °C for 2 min followed by 40 cycles of 98 °C for 15 s, 59 °C for 20 s, and 72 °C for 30 s. Five technical replicates were measured and used to calculate relative quantitative abundances. Next to the samples a non-template control, a non-reverse transcriptase control, and a positive control was set up.

3.3.4. Diversity indices

For a given sample, hybridization results were included only when the sequence counts per sample and taxon were equal to or greater than 2 % of the total sequence counts in the sample. Diversity, richness, evenness and dominance were calculated using the following indices:

Diversity (assesses both richness and evenness): **Simpson index D**

$$D = \sum_{i=1}^{S} pi \;\; x \;\; pi \tag{1}$$

where pi = proportional abundance the i^{th} taxon (share of total PCR product with positive hybridization), S = total number of taxa yielding positive hybridisation. Here we used the reciprocal Simpson diversity index 1/D, which expresses increasing diversity with increasing values.

Richness (number of taxa within a sample): **Menhinick index D_{Mn}**

$$DMn = \frac{S}{\sqrt{N}} \tag{2}$$

where S = number of taxa with positive hybridization, N = number of individuals. i.e. number of total sequence counts with positive hybridization.

Evenness (distribution of abundance within the number of taxa): **Simpson index E**

$$E = \frac{1/D}{S} \tag{3}$$

where D = Simpson diversity index (see above), S = Number of taxa with positive hybridization.

Dominance (proportional abundance of the most abundant taxon within a sample): **Berger-Parker index d**

$$d = N\mathrm{max}/N \tag{4}$$

where Nmax = number of sequence counts of the taxon with the highest hybridization share, N = total abundance (sum of all positive sequence counts).

3.4. Extracellular polymeric substances (EPS)

3.4.1. Isolation of EPS

Total EPS was extracted following Wingender et al. (2001) with slight modifications. Mud samples were suspended in sterile 0.14 M NaCl (1:16 ratio; 1:10 for samples 19,201–21,206), stirred for 60 min at 200 rpm (room temperature), and centrifuged at 20,000 ×*g* for 30 min at 10 °C. Supernatants were filtered twice (0.2 μm cellulose acetate membranes) and stored at −20 °C.

3.4.2. Extraction of DNA

200 μL of isolated EPS solution were used for extraction of DNA by Monarch® PCR & DNA Cleanup Kit (NEB #T1030) according to the manufacturer's instructions. DNA was eluted with 20 μL of nuclease-free water. Total DNA concentration was measured with NanoPhotometer® NP80 (Implen GmbH).

3.4.3. Analysis of proteins

Protein concentrations were determined following Frølund et al. (1996). A total of 700 μL of Lowry reagent - prepared by mixing 0.143 M NaOH and 0.270 M Na_2CO_3 (Solution 1), 0.057 M $CuSO_4$ (Solution 2), and 0.124 M sodium tartrate dihydrate (Solution 3) in a 100:1:1 ratio - was added to 500 μL of EPS extract, vortexed, and incubated for 10 min at room temperature. Subsequently, 100 μL of Folin-Ciocalteu reagent (diluted 0.83:1 with ddH_2O) was added, mixed, and incubated in the dark for 45 min. Absorbance was measured at 750 nm using a NanoPhotometer® NP80.

3.4.4. Analysis of carbohydrates

Determination of carbohydrates was performed according to DuBois et al. (1956). 500 μL of 5 % (*w/v*) phenol solution and 2.5 mL of 100 % sulfuric acid were added to 500 μL EPS solution most quickly and mixed by vortexing After incubation for 10 min at room temperature, samples were incubated for 15 min at 30 °C in a water bath, then for 5 min at

room temperature in the dark. Absorbance was measured at 480 nm (acidic polysaccharides) and 490 nm (neutral polysaccharides) using a NanoPhotometer® NP80.

3.4.5. Analysis of uronic acids

Uronic acids were quantified following Filisetti-Cozzi and Carpita (1991). To 400 µL of EPS extract, 80 µL of Solution 1 (2 M amidosulfonic acid) and 2.36 mL of Solution 2 (0.075 M sodium tetraborate in sulfuric acid) were added, vortexed, and heated at 100 °C for 20 min, followed by 5 min of incubation in an ice bath. 80 µL of Solution 3 (0.15 % 2-phenylphenol in 0.5 % NaOH) was added, vortexed, and incubated for 10 min at room temperature in the dark. Absorbance was measured at 525 nm using a NanoPhotometer® NP80.

3.4.6. Analysis of lipids

Lipids were extracted following Hara and Radin (1978) with minor modifications. 500 µL of n-hexane was added to 500 µL of EPS extract, vortexed vigorously for 30 min at room temperature, then centrifuged at 12,000 ×*g* for 90 s. 400 µL of the upper phase was transferred to a pre-weighed tube, avoiding the interphase. After 24 h of drying the test tube was weighed again and the lipid mass was determined by subtracting the weight of the empty test tube.

All analyses were performed in triplicates. 0.14 M NaCl was used as negative control. All reactions were measured three times. For the determination of proteins, carbon hydrates and uronic acids standard curves were established by performing the respective assay on dilution series of a standard solution of known concentration in triplicates.

4. Results

4.1. Spatial gradients of sediment properties and carbon release

The investigated transect exhibits pronounced spatial gradients in sediment properties (Fig. 2). Here, only the data of the samples that underwent analysis of the microbial community composition are shown, as these were also used for the correlation analyses (Section 4.7). However, this data subset fully reflects the trends observed for the entire data set published earlier (Gebert and Zander, 2024). The spatial gradient of properties related to OM is evidenced by a declining gradient in total organic carbon (TOC) and total nitrogen (TN), carbon from the microbial biomass, paralleled by decreasing rates of aerobic and anaerobic OM mineralization (Fig. 3). Lower CH_4 production rates and higher redox potentials in downstream direction reflect in decreased concentrations in pore dissolved organic carbon (not shown), ammonium, iron and manganese and increased concentrations in phosphate and sulphate. Correspondingly, electrical conductivity of the sediment pore water, indicative of the concentration of dissolved charged components, decreased along the transect. The investigated transect is fully situated in the freshwater regime. North Sea salt intrusion is visible only downstream of approximately river-kilometer 660 (FGG-Elbe, 2018).

Short-term aerobic and anaerobic decay of sediment OM, highlighting the share of easily degradable OM and therefore suited to differentiate sites regarding OM availability, is presented as cumulative C release over a period of 21 days. Sediment OM decay exhibited a pronounced spatial trend with higher C release upstream and lower C release downstream, both when normalized to dry weight (Fig. 3, left panel) and to TOC (Fig. 3, right panel), and both for oxic and anoxic conditions. Aerobic C release exceeded anaerobic C release by an average factor of 4. Higher values of TOC-normalized sediment OM decay indicate increased lability of the OM present in upstream and

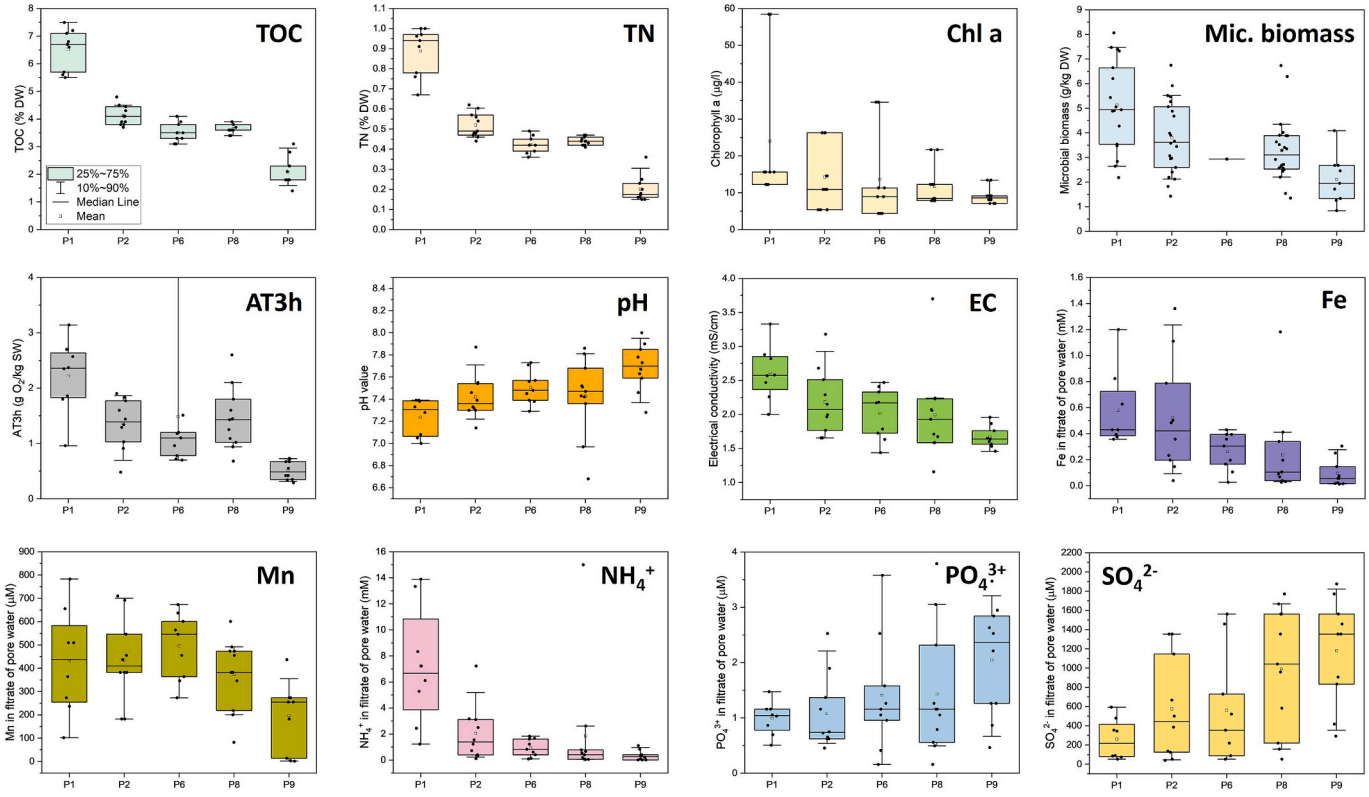

Fig. 2. Selected properties of solids and filtrated pore water at locations along the sampled transect from river km 616 (P1) to 643 (P9, see Fig. 1), collected in 2018–2019. Data include layers FM (fluid mud), PS (pre-consolidated sediment) and CS (consolidated sediment). TOC = Total Organic Carbon, TN = Total Nitrogen, Chl a = Chlorophyll a, AT3h = Oxygen uptake over 3 h, EC = Electrical Conductivity. Number of data per box = 9–11.

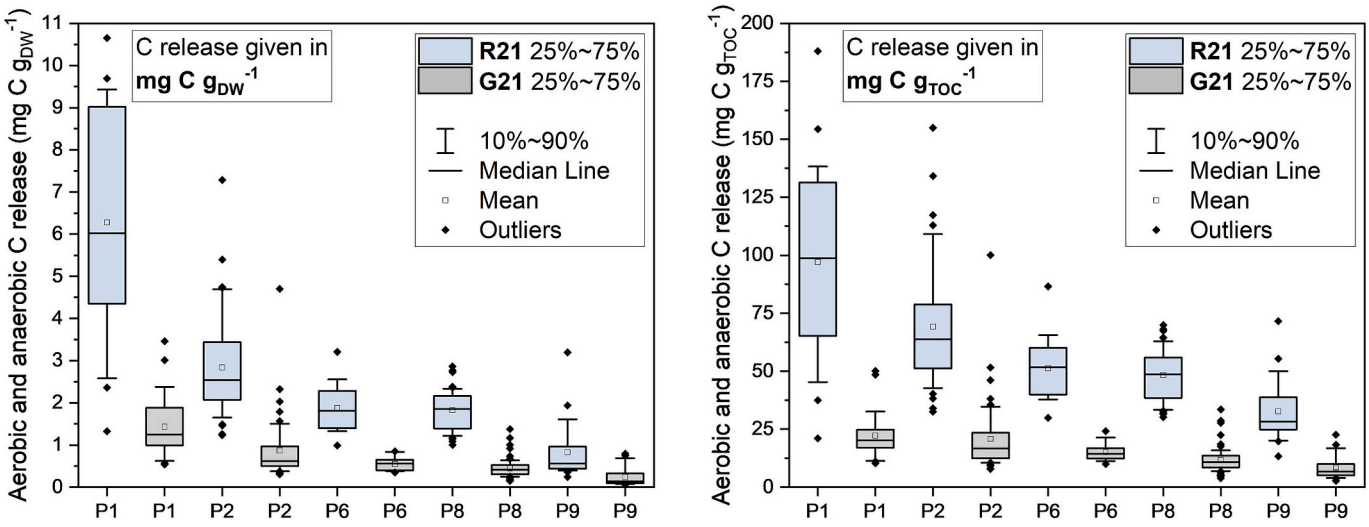

Fig. 3. Aerobic (R, light blue) and anaerobic (G, grey) cumulative C release in 21 days along the sampled transect from river km 616 (P1) to 643 (P9, see Fig. 1). Left = C released normalized to unit dry weight (DW). Right = C release normalized to total organic carbon (TOC). Data include layers FM (fluid mud), PS (pre-consolidated sediment) and CS (consolidated sediment). Data have been published as part of a larger data set by Gebert and Zander (2024).

increased stability in downstream sediment. The largest decease was observed between the most upstream site P1 (river km 616) and the group of all other sites.

4.2. Relative abundance of bacteria, algae and archaea (qPCR)

At all sampling points along the transect, qPCR suggested that bacteria dominate the microbial community (Fig. 1, Supplementary Figs. S1 and S2). Within the PS layer, samples from June displayed a significantly larger share of algae than samples from November, reflecting pronounced seasonal variability of net primary producers. In the case of location P8, the relative abundance of algae in June amounted to a maximum of >25 %. Location P6 was an exception with very similar shares of the individual groups in the PS layer of June and November, although the seasonal variability between June and November becomes evident again in the deeper CS layer (Supplementary Fig. S1). Relative archaeal abundance was very low at all sites (<1 %).

4.3. Composition and diversity of the microbial community

Bacterial and archaeal taxon abundance as well as the ratio of taxon richness to biomass followed clear spatial gradients (Fig. 4) which were also delineated by various of abiotic properties (Fig. 2). As observed for the most abundant bacterial and archaeal taxa (Fig. 4, Supplementary Figs. S3 to S6), the composition of the archaeal community was mostly similar at sites P2, P6, P8, and P9, but markedly different at site P1, the most upstream sampling point also showing the highest sediment OM content and degradability (Figs. 2, 3).

4.3.1. Bacteria

Sequence analysis revealed that 81 % ± 6 % of all bacterial 16S rRNA amplicons belonged to families with a relative abundance of less than 2 %, supportive of a very high phylogenetic diversity. Clear spatial gradients in taxon abundance were detected (Fig. 4, upper panel, Supplementary Figs. S3 and S4. While abundance of species of putative organotrophic *Luteolibacter*, *Dinghuibacter*, *Bacteriodetes* vadinHA17 and *Pirellula* decreased in downstream direction, organotrophic *Chryseolinea*, denitrifying PLTA13 and nitrite oxidizing *Nitrospira* species increased. *Terrimonas* species appeared more evenly distributed. Clearly, the spatial pattern was mainly dominated by site P1 exhibiting a very different bacterial composition, differing most from the ensuing site P2 and sites downstream thereof.

Differential abundance analysis highlights significant changes in relative abundances of all taxa and substantiates the above-mentioned trend that distinct taxa are significantly enriched along the spatial gradient, but also demonstrates that this trend continues beyond the eight most abundant bacterial taxa (see Fig. 5A for top 18 taxa and Supplementary Fig. S7 for top 100 taxa). The most conspicuous taxa in this analysis include *Dinghuibacter (Chitinophagaceae)*, *Halioglobus (Halieaceae)*, *Actibacter (Flavobacteriaceae)*, *Flavobacterium (Flavobacteriaceae)*, and the gammaproteobacterial OM60/NOR5 clade (*Halieaceae*) at P1, *Geothermobacter* (*Geothermobacteraceae*) at P2, *Nitrospira (Nitrospiraceae)* and the unclassified betaproteobacterial glade Ellin6067 at P6, gammaproteobacterial PLTA13 and *Chryseolinea* (*Cytophagaceae*) at P8 as well as uncultured bacterial group TRA3-20, *Vicinamibibacteraceae*, *Sulfurifustis* (*Acidiferrobacteraceae)*, B2M38 and *Woeseia* (*Woesiaceae*) at P9.

4.3.2. Archaea

Methanogenic archaea of the genera *Candidatus* Methanofastidiosum, *Methanoregula* and *Methanosarcina* showed highest relative abundance of 16S rRNA gene amplicons at this sampling point (Fig. 4, middle panel, Supplementary Fig. S6), while further downstream they were less abundant or absent. Contrastingly, these downstream sites were strongly dominated by potential ammonia oxidizing *Nitrosarchaeum* sp. and, to a lesser extent, by *Nitrosopumilus* sp. The highest single individual relative abundance was detected at site P9 where *Nitrosarchaeum* sp. made up 68 % of all archaeal 16S rRNA gene amplicons according to RNA-profiling. High abundance of *Bathyarchaeia* was detected along the entire transect (19 ± 7 %). Marine benthic group D/Deep-Sea Hydrothermal Vent Euryarchaeotic Group 1 (MBG-D/DHVEG-1) showed rather low abundances across all sites, with a few exceptions that do not appear to follow any spatial or seasonal trend (2.3 ± 1.7 %) (Supplementary Fig. S6). Sites P2, P6, P8 and P9, which are subject to regular maintenance dredging, showed little variation with depth (and hence age) while this was more pronounced for the undisturbed upstream site P1.

Differential abundance analyses of archaea revealed that the beforementioned trends of enrichment of methanogens *Methanosarcina*, *Methanoregula*, *Methanosaeta* and *Candidatus* Methanofastidiosum at site P1 and the downstream enrichment of *Nitrosarchaeum* are indeed statistically significant (Fig. 5B). Relative abundance of anaerobic methane oxidizers of the *Methanoperedenaceae,* namely the genera *Methanimicrococcus* and *Candidatus* Methanoperedens increase significantly

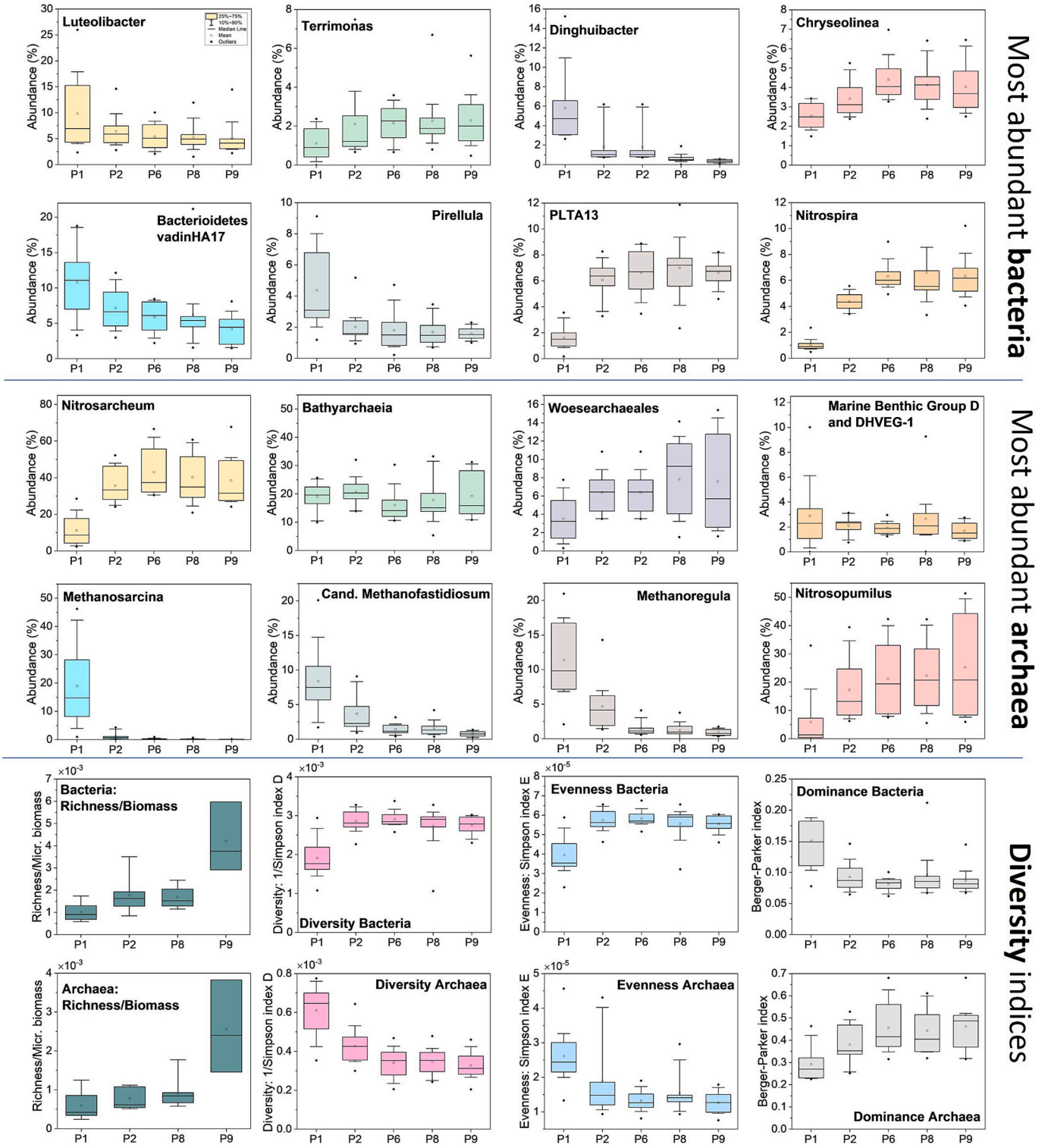

Fig. 4. Share (%) of the eight most abundant bacterial (top) and archaeal (middle) taxa as well as diversity indices (bottom; richness normalized to microbial biomass, diversity, evenness and dominance) at sampling sites P1, P2, P6, P8 and P9.

from the undisturbed upstream site P1 in the downstream direction over P2, P6, P8 and P9 (Fig. 5B, Supplementary Figs. S5 and S6).

4.4. Microbial diversity, richness, evenness and dominance

Diversity and evenness of the bacterial community were lowest at the most upstream site P1 (Fig. 4, upper part lower panel), consequently dominance was highest at site P1. No clear spatial pattern emerged for taxon richness (not shown); however, when taxon richness was normalized to microbial biomass, a clear pattern with lowest bacterial richness at the upstream site P1 and the highest bacterial richness at site P9 emerged. The indices for archaeal diversity, evenness and dominance (lower part of lower panel) revealed an inverse pattern with markedly increased diversity and evenness, but lowest dominance at the most upstream site P1. Also, for archaea, taxon richness was similar across the transect (not shown), but per unit microbial biomass richness increased

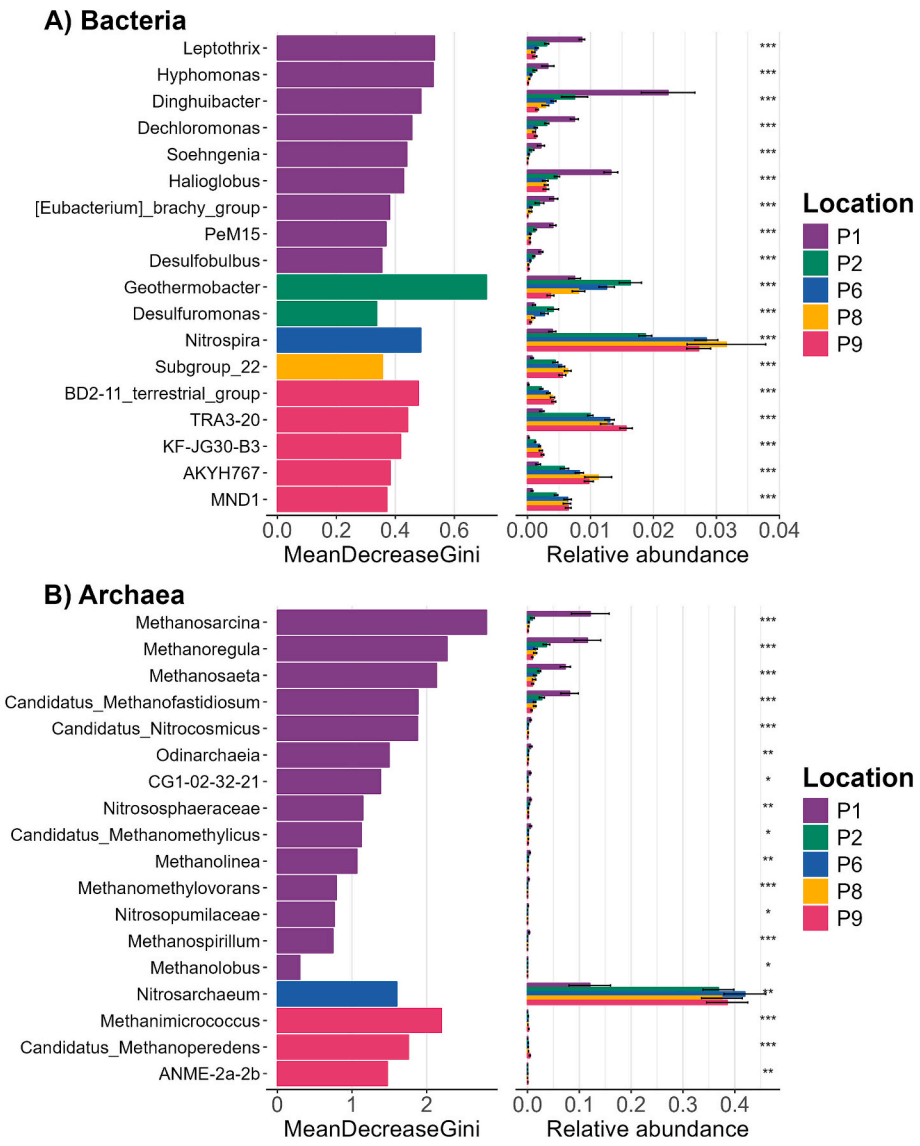

Fig. 5. Differential abundance analysis of bacterial (A) and archaeal (B) taxa at the genus level across all layers. The left panels show the Mean Decrease in the Gini Index, indicating the importance of each taxon in the Random Forest classification. The right panels show the relative abundance of taxa. Only the top 18 taxa with significant changes in relative abundance are shown, with *p*-values marked by asterisks (* <0.05, ** <0.01 and *** <0.001). Sites are color-coded: P1 (purple), P2 (green), P6 (blue), P8 (yellow), and P9 (pink). The analysis was performed using Random-Forest (rf) algorithm in R with the microeco package (Liu et al., 2021) and no p-value adjustment. Samples were rarefied to 2000 and 4000 sequences per sample for bacteria and archaea, respectively.

along the transect.

4.5. *(Dis)similarity of microbial community composition*

The general origin of the deposited sediment appears to be one of the primary factors for determining the bacterial and archaeal community composition (Supplementary Fig. S8 A and B, respectively). Samples from the Port of Rotterdam, influenced by North Sea salinity (PoR), and from Rostock (HRo), reflecting conditions of the Baltic Sea sediments, were included as external reference samples. It is seen that community composition in sediments from the tidal Elbe River in the area of Hamburg indeed differs significantly compared to these external reference locations. Within the sample collective from Hamburg, location P1 stands out with a bacterial and archaeal taxa distribution distinctly different from the other locations, the latter clustering together. With respect to bacteria, site P2 forms another rather separate cluster. For both archaea and bacteria, November samples cluster more closely, indicating larger community similarity between the different locations (Supplementary Fig. S8 C and D, respectively). The month of June 2018, but also October 2018, shows a clearly distinct cluster for bacteria, suggesting relevance of seasonal effects for community differentiation (Supplementary Fig. S8 C). This seasonality is also reflected in the cell numbers (Supplementary Fig. S1). For archaea, a pronounced seasonal effect is seen for the month of October with a community distinctly different from the other months, likely largely related to temperature (Supplementary Fig. S8 D). Archaea in the suspended particulate matter samples, which more frequently exhibit positive redox potentials, cluster most closely, while the deeper consolidated (CS) layers which are constantly subjected to reducing conditions, appear to be the most diverse, whereas bacteria cluster least in SPM layers (Supplementary Fig. S8 E and F, respectively).

4.6. *Extracellular polymeric substances (EPS)*

Lipids represented the bulk mass of microbial EPS along the transect, followed by acid polysaccharides and proteins (Fig. 6). Polysaccharides

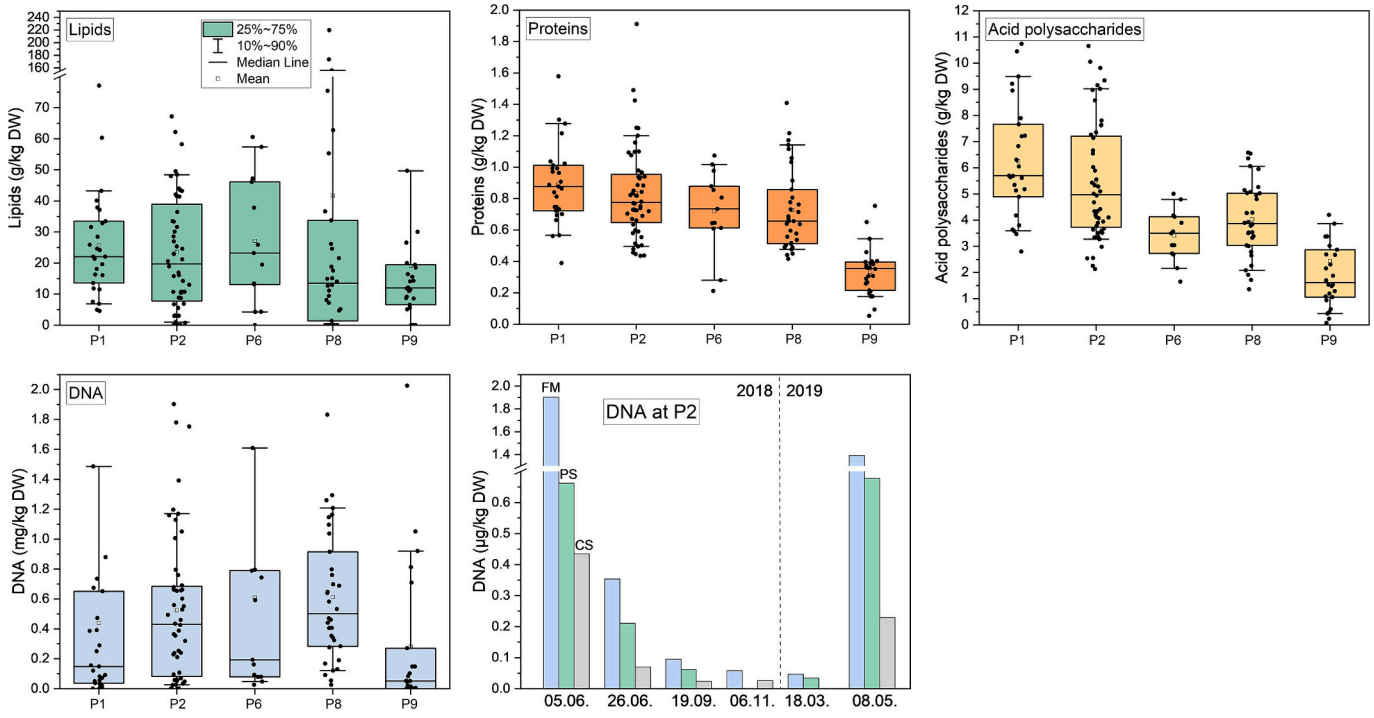

Fig. 6. Concentration of EPS components at sampling sites P1, P2, P6, P8 and P9.

Table 1

Pearson's correlation coefficient for the abundance of bacterial taxa and sediment properties reflecting OM quantity and quality. Bold font: Parameter explains more than 50 % of taxon variability. Threshold for statistical significance of Pearson's r for a two-sided test and $p < 0.01$ = I0.32I, for $\delta^{13}C$ = I0.50I, for DOC in water extract = I0.64I. ns = not significant. Blue shading = positive correlation, red shading = negative correlation. dw = dry weight.

	Taxon	AE pools	AN pools	$\delta^{13}C$	TOC	TOC/S	TOC in < 20 µm	DOC water extract
		mg C / g dw	mg C/ g dw	‰	% dw	-	% dw	g C/ kg dw
Most abundant	*Luteolibacter*	0.32	0.5	-0.32	0.41	0.38	0.41	ns
	Terrimonas	-0.53	ns	0.32	ns	ns	ns	ns
	Dinghuibacter	**0.82**	0.45	**-0.72**	0.7	0.61	**0.71**	ns
	Chryseolinea	-0.66	ns	0.58	-0.39	-0.4	-0.49	ns
	Bacterioidetes vadinHA17	0.63	ns	**-0.8**	0.37	0.5	0.51	**0.95**
	Pirellula	**0.72**	0.63	ns	0.64	0.52	0.53	ns
	PLTA13	**-0.91**	-0.69	0.6	**-0.75**	-0.69	**-0.76**	**-0.86**
	Nitrospira	**-0.86**	-0.56	**0.81**	-0.64	-0.6	-0.61	**-0.83**
Other	*Lentimicrobiaceae*	**0.82**	0.59	**-0.88**	**0.76**	**0.76**	**0.76**	**0.97**
	PHOS-HE36	**0.98**	0.63	**-0.88**	**0.79**	**0.77**	**0.83**	**0.87**
	Subgroup_22	**-0.82**	-0.64	**0.75**	**-0.75**	-0.68	**-0.72**	-0.69
	MND1	**-0.88**	-0.64	**0.75**	**-0.77**	-0.68	**-0.73**	**-0.79**
	Halioglobus	**0.91**	0.69	-0.7	**0.83**	**0.8**	**0.85**	**0.85**
	MBNT15	**-0.81**	-0.61	0.52	**-0.75**	-0.56	-0.65	**-0.85**
	Actibacter	**0.91**	0.65	**-0.91**	**0.82**	**0.69**	**0.83**	**0.76**
	AKYH767	**-0.85**	-0.55	**0.79**	-0.63	-0.57	-0.62	**-0.75**
	Cyanobium_PCC-6307	**0.8**	0.37	-0.52	0.61	0.45	0.6	**0.89**
	Sulfurifustis	**-0.84**	-0.6	0.66	-0.69	-0.59	-0.66	**-0.85**
	B2M28	**-0.86**	-0.43	0.43	-0.52	-0.42	-0.46	-0.69
	Latescibacterota	**-0.9**	-0.45	0.67	-0.56	-0.49	-0.49	ns
	TRA3-20	**-0.86**	-0.6	**0.84**	**-0.75**	**-0.7**	**-0.74**	**-0.87**
	OM60(NOR5)_clade	**0.89**	**0.74**	-0.48	**0.78**	**0.76**	**0.81**	**0.8**
	Ellin6067	**-0.8**	-0.45	0.67	-0.53	-0.51	-0.59	ns
	OM190	**-0.8**	ns	ns	ns	ns	-0.33	ns
Diversity indices	Diversity	**-0.85**	-0.55	**0.68**	-0.59	-0.68	**-0.71**	**-0.85**
	Richness	**-0.77**	ns	0.48	ns	-0.26	ns	ns
	Evenness	**-0.8**	**-0.56**	0.67	**-0.61**	-0.69	**-0.73**	**-0.86**
	Dominance	**0.72**	0.52	-0.66	0.57	0.66	**0.73**	**0.94**

and proteins, biosynthesized in response to microbial metabolic needs and environmental conditions, exhibited a declining gradient in downstream direction, reflecting the spatial pattern observed for TOC, TN, microbial biomass (Fig. 2) and OM turnover (Fig. 3). In contrast, lipids were more evenly distributed along the transect, likely in relation to their chemical stability. Temporal variability of EPS components was most pronounced for EPS-bound DNA (Fig. 6, lower right panel), exhibiting a seasonal re-peak, exemplifying the relation between microbial activity and seasonally varying environmental factors (e.g. temperature) as well as availability of degradable OM, declining with depth (FM towards CS).

4.7. Correlation of community composition with sediment properties

In this section, we present results of pairwise linear correlation analyses between individual environmental parameters and individual taxon abundance and microbial diversity parameters, with each relationship being independent of other measured variables and potential confounding factors.

4.7.1. Bacteria

Bacterial diversity, richness and evenness were all strongly negatively related to the aerobically available degradable OM (AE pools, Table 1) while higher shares of available OM favoured higher dominance. A similar pattern is shown for the water extractable dissolved organic carbon (DOC), and the concentration of TOC in the medium silt and smaller fraction (< 20 μm), which is likely situated in greater physical vicinity to microbiota than larger sized organic particles which are part of the bulk TOC.

Abundance of most taxa was strongly negatively correlated to TOC, DOC and the total share of aerobically degradable carbon (AE pools). Exceptions to this were for *Dinghuibacter*, *Pirellula*, *Lentimicrobiacaeae*, PHOS-HE36, *Halioglobus*, *Actibacter*, *Cyanobium* and OM60 clade, showing a strong positive relation (Table 1). While the nature of the correlation was the same for the aerobically (AE) and anaerobically (AN) available OM, a significantly lower Pearson's r was found for the anaerobically available OM. This indicates that under the mostly anaerobic conditions prevailing in situ (Gebert and Zander, 2024), other parameters than available OM are relevant for taxon abundance. Noteworthy, is that the most abundant taxa (Fig. 4) such as *Luteolibacter* (*Verrucomicrobiaceae*) or *Bacterioidetes* were not necessarily the ones that showed the highest relation to the degradable OM pools, but high correlation coefficients were found also in the group of the less abundant taxa ('Other' in Table 1). Pearson's r assumed inverted values for the parameter $\delta^{13}C$ compared to degradable OM (AE and AN pools), corroborating the previously described lower degradability of sediment OM enriched in the heavy isotope ^{13}C (Zander et al., 2023). Taxa for which a negative relation to degradable OM pools was found showed a positive value for Pearson's r when correlated with $\delta^{13}C$.

The taxa for which a relationship to sediment properties reflecting OM quality and quantity was found were also subjected to a correlation analysis regarding inorganic parameters (see supplementary materials). With respect to the macro-parameter, it is seen that higher Ca (solids) and higher porewater nitrogen (TN) concentrations correlate negatively with bacterial diversity and evenness but positively with bacterial dominance. The same applies to Cd in the sediment's fine fraction <20 μm, however, Cr in this fraction was positively related to diversity and evenness and negatively to dominance. Among the most abundant taxa, the strong positive correlation of *Bacteriodetes* to pore water nitrogen is striking, especially as this was not found for any other taxon, highlighting their likely strong role in OM decay. Additionally, the negative relation of PLTA13 abundance to most metals in the fine fraction, except for Cr (positive), is noteworthy. Also, the other taxa show a differential pattern of correlation to the concentration of metals, with abundances of *Lentimicrobiaceae*, PHOS-HE36 and *Actibacter* responding very similar.

Statistically significant relationships to any other bulk solids or pore water properties were not detected.

4.7.2. Archaea

In spite of the predominantly negative redox potentials and hence anoxic conditions prevailing in the sediment (Gebert and Zander, 2024), archaeal diversity indices showed an only weak positive relation to the sum of the anaerobically available OM (AN pools in Table 2). Contrastingly, diversity and evenness were positively and dominance negatively correlated to aerobically available OM (AE pools). This reflects an opposite pattern of correlation than found for bacteria (Table 1) for all diversity indices. A rather strong positive relationship of diversity and evenness was also found for TOC in the fraction <20 μm, stronger than for bulk TOC itself. Further, these indices also correlated positively with the water-extractable carbon, reflecting the soluble OM not yet tightly bound to the mineral phase and considered more easily accessible to microbial decay (Straathof et al., 2014; Zander et al., 2023).

Although *Bathyarchaeia* exhibited high relative abundances across all sampling sites (Fig. 4, mid panel), their abundance neither followed a spatial gradient nor was it related to any of the parameters reflecting OM quantity, quality and decay. In contrast, the methanogenic archaea *Methanosarcina* (aceticlastic, methylotrophic and hydrogenotrophic methanogenesis), *Candidatus* Methanofastidiosum (methylotrophic) and *Methanoregula* (hydrogenotrophic and methylotrophic methanogenesis), exhibited strong positive relations to the aerobically available OM pools, and to TOC particularly in the fraction <20 μm. Strikingly high values for Pearson's r were found for abundance of these taxa and water-extractable DOC, while the relation was negative to $\delta^{13}C$. The positive relation to the ratio TOC/S was stronger than to TOC, suggesting possible competition between methanogenesis and availability of sulphate as terminal electron acceptor, the latter increasing in downstream direction (Fig. 2).

Also, the less abundant taxa ('Other') mostly exhibited very strong positive correlations to water extractable DOC, always stronger relations to TOC in the fraction <20 μm when compared to bulk TOC and inverse relationships to the concentration of ^{13}C, suggesting reduced degradability of older, already degraded OM enriched in ^{13}C. In this group of taxa, *Methanomethylovorans* stood out with very high correlations to the investigated properties, including a higher correlation of taxon abundance to the ratio of TOC to S than to TOC. This group is known to produce methane from methanol and methylated compounds (e.g. Lomans et al., 1999).

Additionally to the parameters reflecting OM quantity, quality and degradability, correlation analyses comprised a multitude of measured abiotic properties of pore water and solids. However, no patterns explaining archaeal abundance were found. Exceptions are the strong positive relationships between taxa belonging to the *Methanomicrobia* (*Methanosarcina*, *Candidatus* Methanofastidiosum, *Methanoregula*, *Methanomethylovorans*, *Methanolinea*, *Candidatus* Methanomethylicus and *Methanosaeta*), showing strong correlations to the concentration of heavy metals in the fraction <20 μm. We assume this to be a pseudo-correlation as these metals are present in higher concentration in the upstream part of the transect where also the share of degradable OM (Fig. 3) is higher.

5. Discussion

5.1. Spatial gradients of sediment properties and OM lability

OM feed into the investigated system follows a pronounced spatial gradient (Zander et al., 2023; Zander et al., 2022) with the upstream, non-tidal and shallow river section providing more labile, easily degradable OM from primary production into the investigation area. Here, increased depth and turbulence have been shown to promote decay of algal biomass and enhancement of zooplankton grazing (Schöl et al., 2014), leading to the accumulation of phytoplankton-derived N-rich dead biomass in the sediment. This interpretation was previously

Table 2
Pearson's correlation coefficient for the abundance of archaeal taxa and sediment properties reflecting OM quantity and quality. Bold font: Parameter explains more than 50 % of taxon variability. Threshold for statistical significance of Pearson's r for a two-sided test and $p < 0.01$ = I0.32I, for $\delta^{13}C$ = I0.50I, for DOC in water extract = I0.64I. ns = not significant. Blue shading = positive correlation, red shading = negative correlation. dw = dry weight.

	Taxon	AE pools	AN pools	$\delta^{13}C$	TOC	TOC/S	TOC in < 20 μm	DOC water extract
		mg C/ g DW	mg C/ g DW	‰	% dw	-	% dw	g C/ kg dw
Most abundant	*Nitrosarchaeum*	**-0.82**	-0.49	**0.78**	0.54	-0.61	-0.62	**-0.71**
	Bathyarchaeia	ns	ns	ns	ns	ns	ns	ns
	Woesearchaeales	-0.52	-0.42	ns	-0.39	-0.44	ns	ns
	Ca. Nitrosopumilus	-0.63	-0.45	ns	-0.45	-0.49	-0.48	**-0.82**
	Methanosarcina	**0.87**	**0.79**	-0.52	**0.72**	**0.87**	**0.79**	**0.88**
	Ca. Methanofastidiosum	**0.82**	0.5	**-0.75**	0.64	**0.67**	**0.71**	**0.96**
	Methanoregula	**0.8**	0.61	**-0.75**	**0.71**	**0.81**	**0.83**	**0.91**
	Marine_Benthic_Group_D_and_DHVEG-1	ns	ns	ns	ns	ns	ns	ns
Other	*Nitrosopumilaceae*	**0.77**	0.54	ns	0.59	0.5	0.62	0.51
	Aenigmarchaeota	ns	ns	-0.68	ns	ns	0.35	**0.85**
	Methanomassiliicoccus	ns	ns	-0.40	0.43	0.5	0.54	**0.74**
	Methanomethylovorans	**0.91**	**0.75**	-0.40	0.68	**0.83**	**0.79**	**0.94**
	CG1-02-32-21	ns	ns	-0.67	0.39	0.52	0.61	**0.86**
	Methanolinea	0.46	ns	**-0.77**	0.44	0.62	0.56	**0.92**
	Ca. Methanomethylicus	ns	ns	**-0.71**	0.35	0.58	0.44	**0.76**
	Odinarchaeia	0.57	ns	-0.66	0.34	0.57	0.44	**0.86**
	Methanosaeta	**0.81**	0.52	**-0.79**	0.7	0.62	**0.81**	**0.94**
Diversity indices	Diversity	**0.89**	0.41	**-0.83**	0.61	0.59	**0.71**	**0.83**
	Richness	ns	ns	ns	ns	ns	ns	ns
	Evenness	**0.75**	0.48	-0.52	0.54	0.41	0.53	**0.79**
	Dominance	**-0.73**	ns	0.59	-0.41	-0.36	-0.48	-0.69

supported by a high correlation between total N and porewater SiO_2 (Gebert and Zander, 2024) and between sediment total N and chlorophyll in the water column (Spieckermann et al., 2022). The lowest ratio of TOC to TN (average TOC/TN = 7.5) at the most upstream location P1 indeed falls well within the range of 4 to 10 reported for algal biomass (Meyers, 1994). Consequently, TOC and even more so TN have been identified as strong predictors of long-term carbon release from sediments in the investigation area (Gebert and Zander, 2024), as well as of oxygen consumption (Spieckermann et al., 2022). Hydrodynamically, location P1 represents the first sedimentation area for suspended material entering the port area from upstream.

Further to a higher content (see TOC in Fig. 2), OM at P1 is also more labile. This is clearly seen when C release is normalized to TOC (Fig. 3, right) with higher values indicating higher degradability of the OM present in the sediment. Analytically, the higher upstream share of more labile OM is not only seen in more aerobic and anaerobic carbon release (CO_2-C and CH_4-C), but also in the higher share of water-extractable carbon, a lower ratio of acid-base to water-extractable sediment OM, a higher share of organic carbon in the low-density fraction and lower $\delta^{13}C$ values, all reflecting a less progressed decay of OM and a lower extent of stabilization in organo-mineral associations (Straathof et al., 2014; Zander et al., 2023). These data suggest P1 to represent a markedly different habitat in terms of sediment OM quantity (see also Fig. 2), quality, and related carbon fluxes. Enhanced rates of OM decay upstream also reflect in increased electrical conductivity of the pore water due to an increased concentration of solutes and in lower upstream pH values, likely resulting from enhanced OM hydrolysis.

5.2. Extracellular polymeric substances

Microbial communities are embedded in a self-produced matrix of extracellular polymeric substances (EPS), composed primarily of polysaccharides, proteins, extracellular DNA (eDNA), and lipids. These biopolymers serve multiple ecological and structural functions across diverse environments, including soils, freshwater systems, marine sediments, and other aquatic habitats. EPS contribute to cell adhesion, surface colonization, nutrient retention, protection against environmental stress, and long-term carbon storage (Flemming et al., 2025). Polysaccharides and proteins are biosynthesized in response to microbial metabolic needs and environmental conditions, hence reflecting microbial activity as influenced by environmental factors such as OM input, oxygen availability, and sediment properties. Acidic polysaccharides, for instance, are vital for microbial adhesion, biofilm stability, and nutrient capture, making them abundant in areas of high microbial density and availability of degradable OM (Flemming and Wingender, 2010). Proteins, particularly enzymes, are directly linked to OM decay as they catalyse the breakdown of complex substrates (Arnosti, 2011). Their spatial distribution therefore plausibly aligns with gradients of microbial biomass and OM decay patterns. Polysaccharide and protein concentrations peaked where OM degradation was most active (site P1), tapering off in less biologically active regions (Fig. 6).

As structural components of cell membranes and long-term carbon storage molecules, lipids are less directly tied to the metabolic activity that drives OM turnover. Unlike polysaccharides and proteins, lipids are not actively produced in response to localized environmental changes. Instead, their distribution reflects the preservation potential and transport dynamics of OM rather than active microbial processes. Further, lipids, particularly those integrated into EPS, may persist over time, accumulate and diffuse within sediment layers due to their hydrophobic nature and low degradation rates in anoxic environments (Wakeham et al., 1997). The low redox potentials in the investigated sediments (Gebert and Zander, 2024) indeed suggest prevalence of anoxic conditions. Altogether, this leads to their relatively uniform distribution across the sedimentary transect (Duteil et al., 2022).

Depth (age) and temporal variations in EPS-bound DNA concentrations exemplify the change of microbial activity over time and with sediment stratification (Nagler et al., 2018). In upper FM layers, where oxygen and OM are more abundant (Fig. 6), microbial activity peaks, leading to higher concentrations of polysaccharides and proteins. Over time, as these layers consolidate and are buried by newly settled material, microbial activity decreases, and EPS concentrations decline. The observed seasonal re-peak of DNA likely reflects cycles of OM input and

microbial growth (e.g., following phytoplankton blooms), further supporting the dynamic interplay between microbial processes and EPS composition.

5.3. Diversity and composition of the microbial community along the spatial gradient

Both the bacterial and the archaeal communities strongly differentiated along the transect (Fig. 5, Supplementary Figs. S7 and S8), aligning with patterns of degradable OM (Fig. 3), reflecting in corresponding gradients of pore water ammonium concentrations, concentrations of solutes (reflected by parameter EC) and pH (Fig. 2). The most extreme sampling point in this regard was the most upstream point P1, while communities at other locations along the transect appeared more similar. Location-driven patterns mostly overruled depth- and time-related variability, as evidenced by principal coordinate analysis (Supplementary Fig. S8). Increased OM availability aligned with decreased bacterial diversity and evenness and, consequently, increased dominance of distinct groups (Fig. 5A, Supplementary Fig. S7). The archaeal community exhibited an inverted pattern, suggesting increased diversity and evenness but reduced dominance with an increased share of degradable OM. Given the mostly negative redox potentials (Gebert and Zander, 2024), in situ OM decay can be assumed to occur under strictly anoxic conditions and therefore to be driven by the archaeal community. Findings of increased archaeal diversity with an increased concentration of degradable OM in the anoxic sediments are paralleled by findings of increased bacterial diversity with increased carbon-normalized respiration in unsaturated soils (Vicena et al., 2022). A positive link between microbial functional diversity in soil and the rate of decomposition of OM was also found by numerical substrate-microbial reaction network modelling (Khurana et al., 2023). In both cases, the positive correlation between diversity and OM degradation was valid when OM decay was limited by substrate availability. Together, this suggests that OM mineralization is limited by availability of microbially degradable OM and not by other parameters.

Bastida et al. (2021) illustrate that the ratio between richness and biomass correlates inversely with transformation rates of organic carbon. The authors highlight the importance of soil organic carbon as the major regulator of the ratio between soil microbial diversity and biomass and conclude that increased diversification of the microbial community in soils at reduced biomass negatively affects critical broad processes such as soil respiration. Along the investigated transect, microbial biomass decreased markedly in downstream direction (Fig. 2), while taxon richness did not stratify between sites. As a consequence, the ratio of taxon richness to biomass increased markedly in downstream direction. As found by Bastida et al. (2021), the ratio is inversely related to OM decay (Fig. 3), corroborating the assumption of a higher share of stabilized OM (Zander et al., 2023) and hence a lower share of microbially accessible OM to control carbon fluxes from the individual sites.

The taxa identified from RNA source material via 16S rRNA genes indicate that microorganisms at P1 are primarily associated with OM degradation. This is consistent with the hydrodynamic patterns in the port, making P1 the first sedimentation area for suspended material imported from upstream with high levels of labile, easily degradable carbon. In particular, a significant increase in the relative abundances of aerobic and facultatively anaerobic organotrophic bacteria was observed at site P1 (Fig. 5A, Supplementary Fig. S7). Most striking here are *Dinghuibacter* of the *Chitinophagacea* (Lv et al., 2016), *Halioglobus* and NOR5/OM60 of the *Halieaceae* (Li et al., 2023; Montecillo, 2024), as well as Actibacter and *Flavobacterium* of the *Flavobacteriaceae* (Gavriilidou et al., 2020; Kim et al., 2008). Members of the genus *Dinghuibacter* have been shown to be a key species for DOM metabolization in river sediments before (Wang et al., 2022). *Haliaceae* species are widely distributed in marine environments and are involved in the decomposition of polysaccharides with phytoplanktonic origin, as evidenced by the diverse set of carbohydrate-active enzymes (CAZymes) found on the genomes of cultured representatives (Li et al., 2023). Here, they thrive in a freshwater environment, which, however, receives sediment import from the sea. Members of the family *Flavobacteriaceae* also possess a broad spectrum of CAZymes, making them specialists in OM degradation capable of utilizing a variety of carbon sources (Silva et al., 2023). Thus, *Flavobacteriaceae* species are renowned for their ability to degrade high molecular weight macromolecules, such as complex polysaccharides and proteins (Gavriilidou et al., 2020 and references therein).

The fact that P1 emerged as hotspot of sediment OM quantity and carbon release is also mirrored by the pronounced abundance of anaerobic methanogenic archaea who gain energy by forming methane from different C1 or C2 compounds that are produced from syntrophic partners as by-products during organic-matter breakdown (Liu and Whitman, 2008). The conventional methanogenic lineages within the *Euryarchaeota* are categorized based on their substrate preference into (i) hydrogenotrophic methanogens that reduce hydrogen (H_2) and CO_2, (ii) aceticlastic methanogenes that use acetate, (iii) methylotrophic methanogens that utilize methylated compounds (X-CH_3) and (iv) H_2-dependent methylotrophic methanogens that metabolize X-CH_3 and H_2 for methane production (Evans et al., 2019). A large variety of methanogenic archaea were found in significantly higher abundances at site P1 (Fig. 5B), including representative species for each of the above-mentioned forms of methanogenesis. Particularly striking here were *Methanosarcina (*Fig. 5B*)* whose members are known for their metabolic versatility, as they can utilize a wide range of substrates for aceticlastic, methylotrophic and hydrogenotrophic methanogenesis (Evans et al., 2019; Lyu et al., 2018). Other methanogenic archaea that thrive better at P1 compared to the more downstream sites P2, P6, P8 and P9 were e.g. *Methanoregula* (hydrogenotrophic and methylotrophic methanogenesis), suggested as a hub methanogen and key predictor of methane fluxes in wetlands (Bechtold et al., 2025), *Methanosaeta (*aceticlastic methanogenesis) (Carr et al., 2018) and *Methanofastidiosum* (methylotrophic methanogenesis) (Nobu et al., 2016) (Fig. 5B, and Supplementary Figs. S5 and S6). This high variety of methanogenic archaea at site P1 suggests a broad substrate spectrum that can be utilized by the local archaeal methanogenic community and thus reflects the presence of diverse metabolic niches within the environmental space of site P1 (Malard and Guisan, 2023).

Methanogenic archaea have been shown to account for more than one-half of the methane produced annually on Earth, demonstrating their crucial role in the global carbon cycle (Evans et al., 2019). Across all sites, depths, and seasons sampled along the Elbe River transect in this study, archaea made up a much smaller proportion of the total microbial community compared to bacteria and microalgae (Fig. 1 and Supplementary Fig. 1). However, in the field, significant in situ methanogenesis was observed, visible through ebullition of gas bubbles from the sediment (Zander, 2022), and significant methanogenic activity measured in the laboratory (Fig. 3), highlighting that even low abundant species can have a significant impact on the ecosystem. Since methanogens are outcompeted by sulfate-reducing bacteria, denitrifying bacteria, and iron-reducing bacteria when electron acceptors other than CO_2 are present (Liu and Whitman, 2008), high methanogenic activity at P1 would suggest limited availability of O_2, NO_3^-, Fe^{3+}, and SO_4^{2-}, indeed aligning with the geochemical features of the sediment pore water at P1 as described above.

For marine sediments it has been estimated that around 90 % of the produced methane is oxidized to CO_2 by archaeal methanotrophs (Hinrichs and Boetius, 2003). At site P1, anaerobic methanotrophic archaea (ANME) were found in low abundances, with *Candidatus* Methanoperedens (ANME2b) related taxa accounting for 0.14 % in June, and *Candidatus* Methanoperedens (ANME2b) and ANME2a-2b related taxa making up 0.11 % and 0.04 %, respectively, in November (Supplementary Figs. S5 and S6). Strictly negative redox potentials and ebullition-driven mass transport of methane, however, preclude

effective oxidation of methane in the sediment or the water column.

A noticeable trend is that the majority of genera exhibiting significantly higher abundances at site P1 gradually decrease along the transect in downstream direction from P2 over P6 and P8 to P9 (Fig. 5). This pattern aligns with the observed OM lability gradient, with a higher proportion of labile OM at the most upstream site P1 and supports the hypothesis that the availability of labile OM is the main factor that directly or indirectly controls the abundance of these species. In contrast, *Nitrosarchaeum* species, among others, show a different distribution pattern. Their abundances are lower at P1, but remain consistently higher at downstream sites P2, P6, P8 and P9 (Figs. 4, 5B). The genus *Nitrosarchaeum* has been described as chemolithoautotrophic, aerobic ammonia-oxidizing archaea (AOA), carrying out oxidation of ammonia to nitrite using oxygen as a terminal electron acceptor (Tolar et al., n.d.). However, AOA have been found to also thrive even in oxygen-depleted environments (Hernández-Magaña and Kraft, 2024, and references therein). Initially, it was believed that AOA were inactive under anoxic conditions, but studies on the AOA isolate *Nitrosopumilus maritimus* revealed that the NO-dismutation pathway was performed to produce dinitrogen and oxygen, with the latter being available for ammonia oxidation (Kraft et al., 2022). Possibly this type of self-provision with O_2 is more widespread within the AOA and gives *Nitrosarchaeum* species the possibility to thrive in the anerobic, ammonium-containing sediments of the Elbe River. Unlike ammonium oxidizing bacteria (AOB), AOA are typically found in habitats with low NH_4^+ concentrations (Ghimire-Kafle et al., 2024). For example, the isolate *Nitrosarchaeum koreense* MY1^T exhibited a maximum tolerance to NH_4^+ of 10 mM (Jung et al., 2018). At site P1, the NH_4^+ concentration was higher than at the downstream sites (Fig. 2), which may explain why *Nitrosarchaeum* is significantly less abundant at P1 and that ammonium concentration is the driving factor.

For bacteria, there is a clear shift downstream of site P1, with an increasing abundance of mixotrophic, autotrophic, and chemotrophic species (5 A). This trend likely reflects the decreased availability of labile OM along the transect, opening niches for metabolically versatile bacteria. For example, *Geothermobacter* are significantly more abundant at sites downstream of P1. *Geothermobacter* are described as a genus of mixotrophic iron(III)-reducers that affect biogeochemical cycling of multiple elements in anoxic environments (Li et al., 2020; Pérez-Rodríguez et al., 2021). Abundances of *Nitrospira* species also increases in the downstream direction along the studied transect (Fig. 5A, Supplementary Fig. S4). Amplicon reads that were assigned to the genus *Nitrospira* are most closely related to four different species, including *Nitrospira moscoviensis* and three unclassified *Nitrospira* species. Traditionally considered as aerobic, chemolithoautotrophic, nitrite oxidizers, *Nitrospira* have been found to possess greater metabolic flexibility than previously recognized. Alongside their primary role in aerobic nitrite oxidation, cultured representatives were found to be able to utilize ammonia (as comammox bacteria), formate and hydrogen as electron donors for aerobic respiration (Daims et al., 2016; Leung et al., 2022). Furthermore, formate and hydrogen can support nitrate respiration under anoxic conditions, allowing *Nitrospira* to endure periodes of nitrite or oxygen depletion (Koch et al., 2015). This metabolic versatility may explain why *Nitrospira* species have established a niche in the mainly anoxic sediments of the Elbe River. The abundance of PLTA13 at sites downstream of P1, but especially at P6, are also significantly higher (Supplementary Figs. S4 and S7). The genus PLTA13 has been attributed a role as heterotrophic denitrifiers, contributing to the stabilization of an anammox consortium by removing excess nitrate from the system (Ma et al., 2022). However, the ecological significance of PLTA13 remains largely unknown and further research is needed to understand their metabolic niche. The abundance of *Woeseia* (*Woeseiaceae*) changes with the gradient along the transect, peaking at the downstream site P9 (Supplementary Figs. S4 and S7). Recognized as one of the most prominent microbial groups in marine sediments, the *Woeseiaceae* are ubiquitously abundant in both coastal sediments and deep-sea surface sediments (Hoffmann et al., 2020), but have been found in estuarine environments as well (Baker et al., 2015). Representatives of the genus *Woeseia* display a rather broad spectrum of physiological traits, with some being obligate chemorganoheterotrophs, while individual genomes recovered from coastal and estuarine sediments indicate the potential for chemolithoautotrophy driven by the oxidation of sulfur- and hydrogen (Baker et al., 2015; Dyksma et al., 2016; Mußmann et al., 2017). The limited knowledge we have of the genus *Woeseia*, primarily consisting of uncultured representatives, makes it difficult to determine the key factor driving their improved adaptation to the habitat conditions prevailing further downstream of the investigated transects. But, bringing new isolates into culture and incorporating metatranscriptomic analyses would lead to a more comprehensive understanding.

6. Conclusions

The marked gradients in OM lability in Elbe River sediment, with a higher share of aerobically and anaerobically available OM upstream and a greater share of stabilized OM downstream, act as key drivers regulating syntrophic microbial community composition and associated metabolic features and processes. Enhanced carbon availability upstream is suggested to invoke a less diverse, more specialized bacterial community, providing a variety of C1-C2-metabolites for subsequent utilization by a highly diverse archaeal community. In contrast, low carbon availability appears to foster metabolic versatility and hence taxon diversity of bacteria but reduces archaeal diversity. The ratio between species richness and biomass, increasing for both bacteria and archaea along the transect appears as a suitable indicator for available carbon, which is corroborated by corresponding spatial patterns of EPS-components that reflect metabolic activity, polysaccharides and proteins. This study provides relevant insights into dynamics of sediment-bound aquatic carbon and the corresponding diversity and functionality of the associated microbial community. The findings enhance understanding of the role of fine-grained, organic-rich fluvial sediments as nexus between the terrestrial to the marine carbon cycle.

CRediT authorship contribution statement

Julia Gebert: Writing – original draft, Visualization, Validation, Supervision, Resources, Project administration, Methodology, Funding acquisition, Formal analysis, Conceptualization. **Stefanie Böhnke-Brandt:** Writing – original draft, Visualization, Validation, Software, Methodology, Investigation, Formal analysis, Conceptualization. **Florian Zander:** Methodology, Investigation, Formal analysis. **Daniela Indenbirken:** Investigation. **Lutgardis Bergmann:** Investigation, Formal analysis. **Ines Krohn:** Writing – review & editing, Resources, Methodology, Formal analysis. **Mirjam Perner:** Writing – review & editing, Resources, Conceptualization.

Funding

This study was funded by Hamburg Port Authority AöR and carried out within the project BIOMUD, part of the MUDNET academic network www.tudelft.nl/mudnet/. Additional financial support for the presented work and its publication was provided through the program-oriented funding (PoF IV, Topic 6) of the Helmholtz Association.

Declaration of competing interest

The authors declare that they have no known competing financial interests or personal relationships that could have appeared to influence the work reported in this paper.

Acknowledgements

Analyses of sediment OM fraction were carried out in collaboration

with Wageningen University & Research, Chair group Soil Chemistry and Chemical Soil Quality (Prof. Dr. Rob Comans). Ronny Baaske is acknowledged for his support with sequence data analysis in R.

Appendix A. Supplementary data

Supplementary data to this article can be found online at https://doi.org/10.1016/j.scitotenv.2025.180614.

Data availability

The 16S rRNA raw data generated in this study was deposited at the Sequence Read Archive of NCBI (National Center for Biotechnology Information) under the BioProject ID PRJNA1267126.

References

Amaral-Zettler, L.A., McCliment, E.A., Ducklow, H.W., Huse, S.M., 2009. A method for studying protistan diversity using massively parallel sequencing of V9 hypervariable regions of small-subunit ribosomal RNA genes. PloS One 4 (7), e6372.

Arnosti, C., 2011. Microbial extracellular enzymes and the marine carbon cycle. Ann. Rev. Mar. Sci. 3, 401–425.

Baker, B.J., Lazar, C.S., Teske, A.P., Dick, G.J., 2015. Genomic resolution of linkages in carbon, nitrogen, and sulfur cycling among widespread estuary sediment bacteria. Microbiome 3.

Bastida, F., Eldridge, D.J., Garcia, C., Kenny Png, G., Bardgett, R.D., Delgado-Baquerizo, M., 2021. Soil microbial diversity-biomass relationships are driven by soil carbon content across global biomes. ISME J. 15 (7), 2081–2091.

Bechtold, E.K., Ellenbogen, J.B., Villa, J.A., de Melo Ferreira, D.K., Oliverio, A.M., Kostka, J.E., Rich, V.I., Varner, R.K., Bansal, S., Ward, E.J., Bohrer, G., Borton, M.A., Wrighton, K.C., Wilkins, M.J., 2025. Metabolic interactions underpinning high methane fluxes across terrestrial freshwater wetlands. Nat. Commun. 16 (1), 944.

Bolyen, E., Rideout, J.R., Dillon, M.R., Bokulich, N.A., Abnet, C.C., Al-Ghalith, G.A., Alexander, H., Alm, E.J., Arumugam, M., Asnicar, F., Bai, Y., Bisanz, J.E., Bittinger, K., Brejnrod, A., Brislawn, C.J., Brown, C.T., Callahan, B.J., Caraballo-Rodriguez, A.M., Chase, J., Cope, E.K., Da Silva, R., Diener, C., Dorrestein, P.C., Douglas, G.M., Durall, D.M., Duvallet, C., Edwardson, C.F., Ernst, M., Estaki, M., Fouquier, J., Gauglitz, J.M., Gibbons, S.M., Gibson, D.L., Gonzalez, A., Gorlick, K., Guo, J., Hillmann, B., Holmes, S., Holste, H., Huttenhower, C., Huttley, G.A., Janssen, S., Jarmusch, A.K., Jiang, L., Kaehler, B.D., Kang, K.B., Keefe, C.R., Keim, P., Kelley, S.T., Knights, D., Koester, I., Kosciolek, T., Kreps, J., Langille, M.G.I., Lee, J., Ley, R., Liu, Y.X., Loftfield, E., Lozupone, C., Maher, M., Marotz, C., Martin, B.D., McDonald, D., McIver, L.J., Melnik, A.V., Metcalf, J.L., Morgan, S.C., Morton, J.T., Naimey, A.T., Navas-Molina, J.A., Nothias, L.F., Orchanian, S.B., Pearson, T., Peoples, S.L., Petras, D., Preuss, M.L., Pruesse, E., Rasmussen, L.B., Rivers, A., Robeson 2nd, M.S., Rosenthal, P., Segata, N., Shaffer, M., Shiffer, A., Sinha, R., Song, S.J., Spear, J.R., Swafford, A.D., Thompson, L.R., Torres, P.J., Trinh, P., Tripathi, A., Turnbaugh, P.J., Ul-Hasan, S., van der Hooft, J.J.J., Vargas, F., Vazquez-Baeza, Y., Vogtmann, E., von Hippel, M., Walters, W., et al., 2019. Reproducible, interactive, scalable and extensible microbiome data science using QIIME 2. Nat. Biotechnol. 37 (8), 852–857.

Bradley, I.M., Pinto, A.J., Guest, J.S., 2016. Design and evaluation of Illumina MiSeq-compatible, 18S rRNA gene-specific primers for improved characterization of mixed phototrophic communities. Appl. Environ. Microbiol. 82 (19), 5878–5891.

Callahan, B.J., McMurdie, P.J., Rosen, M.J., Han, A.W., Johnson, A.J.A., Holmes, S.P., 2016. DADA2: high-resolution sample inference from Illumina amplicon data. Nat. Methods 13 (7), 581.

Carr, S.A., Schubotz, F., Dunbar, R.B., Mills, C.T., Dias, R., Summons, R.E., Mandernack, K.W., 2018. Acetoclastic Methanosaeta are dominant methanogens in organic-rich Antarctic marine sediments. ISME J. 12 (2), 330–342.

Cerqueira, T., Pinho, D., Froufe, H., Santos, R.S., Bettencourt, R., Egas, C., 2017. Sediment microbial diversity of three deep-sea hydrothermal vents southwest of the Azores. Microb. Ecol. 74 (2), 332–349.

Daims, H., Lucker, S., Wagner, M., 2016. A new perspective on microbes formerly known as nitrite-oxidizing Bacteria. Trends Microbiol. 24 (9), 699–712.

Deng, Z., He, Q., Safar, Z., Chassagne, C., 2019. The role of algae in fine sediment flocculation: in-situ and laboratory measurements. Mar. Geol. 413, 71–84.

Ding, J., Zhang, Y., Wang, H., Jian, H., Leng, H., Xiao, X., 2017. Microbial community structure of deep-sea hydrothermal vents on the ultraslow spreading southwest Indian ridge. Front. Microbiol. 8, 1012.

DuBois, M., Gilles, K.A., Hamilton, J.K., Rebers, P.A., Smith, F., 1956. Colorimetric method for determination of sugars and related substances. Anal. Chem. 28 (3), 350–356.

Duteil, T., Bourillot, R., Braissant, O., Gregoire, B., Leloup, M., Portier, E., Brigaud, B., Fenies, H., Svahn, I., Henry, A., Yokoyama, Y., Visscher, P.T., 2022. Preservation of exopolymeric substances in estuarine sediments. Front. Microbiol. 13, 921154.

Dyksma, S., Bischof, K., Fuchs, B.M., Hoffmann, K., Meier, D., Meyerdierks, A., Pjevac, P., Probandt, D., Richter, M., Stepanauskas, R., Mussmann, M., 2016. Ubiquitous Gammaproteobacteria dominate dark carbon fixation in coastal sediments. ISME J. 10 (8), 1939–1953.

Evans, P.N., Boyd, J.A., Leu, A.O., Woodcroft, B.J., Parks, D.H., Hugenholtz, P., Tyson, G. W., 2019. An evolving view of methane metabolism in the Archaea. Nat. Rev. Microbiol. 17 (4), 219–232.

FGG-Elbe, 2018. A-Bericht national der Flussgebietsgemeinschaft Elbe in: Schnellbericht zur Probenahme vom 06.02.2018. https://www.fgg-elbe.de/files/Download-Archive/Gewaesserguete/Schnellberichte%20Befliegung_ab_2014/181113_Schnellbericht_Befliegung.pdf. Accessed 13 August 2025, Längsprofil Tiedeelbe - Bericht Nr. 1/2018.

Filisetti-Cozzi, T.M.C.C., Carpita, N.C., 1991. Measurement of uronic acids without interference from neutral sugars. Anal. Biochem. 197 (1), 157–162.

Flemming, H.C., Wingender, J., 2010. The biofilm matrix. Nat. Rev. Microbiol. 8 (9), 623–633.

Flemming, H.C., van Hullebusch, E.D., Little, B.J., Neu, T.R., Nielsen, P.H., Seviour, T., Stoodley, P., Wingender, J., Wuertz, S., 2025. Microbial extracellular polymeric substances in the environment, technology and medicine. Nat. Rev. Microbiol. 23 (2), 87–105.

Frølund, B., Palmgren, R., Keiding, K., Nielsen, P.H., 1996. Extraction of extracellular polymers from activated sludge using a cation exchange resin. Water Res. 30 (8), 1749–1758.

Gavriilidou, A., Gutleben, J., Versluis, D., Forgiarini, F., van Passel, M.W.J., Ingham, C.J., Smidt, H., Sipkema, D., 2020. Comparative genomic analysis of *Flavobacteriaceae*: insights into carbohydrate metabolism, gliding motility and secondary metabolite biosynthesis. BMC Genomics 21 (1), 569.

Gebert, J., Zander, F., 2024. Aerobic and anaerobic mineralisation of sediment organic matter in the tidal river Elbe. J. Soil. Sediment. 24 (7), 2874–2886.

Ghimire-Kafle, S., Weaver Jr., M.E., Kimbrel, M.P., Bollmann, A., 2024. Competition between ammonia-oxidizing archaea and complete ammonia oxidizers from freshwater environments. Appl. Environ. Microbiol. 90 (3), e0169823.

Groengroeft, A., Jaehnig, U., Miehlich, G., Lueschow, R., Maass, V., Stachel, B., 1998. Distribution of metals in sediments of the Elbe estuary in 1994. Water Sci. Technol. 37 (6–7), 109–116.

Hara, A., Radin, N.S., 1978. Lipid extraction of tissues with a low-toxicity solvent. Anal. Biochem. 90 (1), 420–426.

Hernández-Magaña, E., Kraft, B., 2024. Nitrous oxide production and consumption by marine ammonia-oxidizing archaea under oxygen depletion. Front. Microbiol. 15, 1410251.

Hinrichs, K.U., Boetius, A., 2003. The anaerobic oxidation of methane: new insights in microbial ecology and biogeochemistry. In: Wefer, G., Billett, D., Hebbeln, D., Jørgensen, B.B., Schlüter, M., Van Weering, T.C.E. (Eds.), Ocean Margin Systems. Springer Berlin Heidelberg, pp. 457–477.

Hoffmann, K., Bienhold, C., Buttigieg, P.L., Knittel, K., Laso-Perez, R., Rapp, J.Z., Boetius, A., Offre, P., 2020. Diversity and metabolism of *Woeseiales* bacteria, global members of marine sediment communities. ISME J. 14 (4), 1042–1056.

Jommi, C., Muraro, S., Trivellato, E., Zwanenburg, C., 2019. Experimental results on the influence of gas on the mechanical response of peats. Geotechnique 69 (9), 753–766.

Jung, M.Y., Islam, M.A., Gwak, J.H., Kim, J.G., Rhee, S.K., 2018. *Nitrosarchaeum koreense* gen. nov., sp. nov., an aerobic and mesophilic, ammonia-oxidizing archaeon member of the phylum Thaumarchaeota isolated from agricultural soil. Int. J. Syst. Evol. Microbiol. 68 (10), 3084–3095.

Kaehler, B.D., Bokulich, N.A., McDonald, D., Knight, R., Caporaso, J.G., Huttley, G.A., 2019. Species abundance information improves sequence taxonomy classification accuracy. Nat. Commun. 10 (1), 4643.

Keil, R.G., Mayer, L.M., Turekian, K.K., 2014. 12.12 - mineral matrices and organic matter. In: Holland, H.D. (Ed.), Treatise on Geochemistry, Second edition. Elsevier, pp. 337–359.

Khurana, S., Abramoff, R., Bruni, E., Dondini, M., Tupek, B., Guenet, B., Lehtonen, A., Manzoni, S., 2023. Interactive effects of microbial functional diversity and carbon availability on decomposition – a theoretical exploration. Ecol. Model. 486, 110507.

Kim, J.H., Kim, K.Y., Hahm, Y.T., Kim, B.S., Chun, J., Cha, C.J., 2008. Actibacter sediminis gen. nov., sp. nov., a marine bacterium of the family Flavobacteriaceae isolated from tidal flat sediment. Int. J. Syst. Evol. Microbiol. 58 (Pt 1), 139–143.

Klindworth, A., Pruesse, E., Schweer, T., Peplies, J., Quast, C., Horn, M., Glockner, F.O., 2013. Evaluation of general 16S ribosomal RNA gene PCR primers for classical and next-generation sequencing-based diversity studies. Nucleic Acids Res. 41 (1), e1.

Koch, H., Lucker, S., Albertsen, M., Kitzinger, K., Herbold, C., Spieck, E., Nielsen, P.H., Wagner, M., Daims, H., 2015. Expanded metabolic versatility of ubiquitous nitrite-oxidizing bacteria from the genus Nitrospira. Proc. Natl. Acad. Sci. U. S. A. 112 (36), 11371–11376.

Kraft, B., Jehmlich, N., Larsen, M., Bristow, L.A., Konneke, M., Thamdrup, B., Canfield, D.E., 2022. Oxygen and nitrogen production by an ammonia-oxidizing archaeon. Science 375 (6576), 97–100.

Leung, P.M., Daebeler, A., Chiri, E., Hanchapola, I., Gillett, D.L., Schittenhelm, R.B., Daims, H., Greening, C., 2022. A nitrite-oxidising bacterium constitutively consumes atmospheric hydrogen. ISME J. 16 (9), 2213–2219.

Li, X.M., Ding, L.J., Li, X.M., Zhu, Y.G., 2020. Abundance, diversity, and structure of *Geobacteraceae* community in paddy soil under long-term fertilization practices. Appl. Soil Ecol. 153.

Li, S.H., Kang, I., Cho, J.C., 2023. Metabolic versatility of the family *Halieaceae* revealed by the genomics of novel cultured isolates. Microbiol. Spectr. 11 (2), e0387922.

Liu, Y., Whitman, W.B., 2008. Metabolic, phylogenetic, and ecological diversity of the methanogenic archaea. Ann. N. Y. Acad. Sci. 1125, 171–189.

Liu, C., Cui, Y., Li, X., Yao, M., 2021. Microeco: an R package for data mining in microbial community ecology. FEMS Microbiol. Ecol. 97 (2).

Lomans, B.P., Maas, R., Luderer, R., Op den Camp, H.J., Pol, A., van der Drift, C., Vogels, G.D., 1999. Isolation and characterization of *Methanomethylovorans hollandica* gen. Nov., sp. nov., isolated from freshwater sediment, a methylotrophic

methanogen able to grow on dimethyl sulfide and methanethiol. Appl. Environ. Microbiol. 65 (8), 3641–3650.
Lv, Y.Y., Wang, J., Chen, M.H., You, J., Qiu, L.H., 2016. *Dinghuibacter silviterrae* gen. Nov., sp. nov., isolated from forest soil. Int. J. Syst. Evol. Microbiol. 66 (4), 1785–1791.
Lyu, Z., Shao, N., Akinyemi, T., Whitman, W.B., 2018. Methanogenesis. Curr. Biol. 28 (13), R727–R732.
Ma, J., Wang, K., Shi, C., Liu, Y., Yu, C., Fang, K., Fu, X., Yuan, Q., Zhou, Y., Gong, H., 2022. A novel anammox aggregate nourished sustainably internal heterotrophic nitrate removal pathway with endogenous carbon source. Bioresour. Technol. 346, 126525.
Malard, L.A., Guisan, A., 2023. Into the microbial niche. Trends Ecol. Evol. 38 (10), 936–945.
Malarkey, J., Baas, J.H., Hope, J.A., Aspden, R.J., Parsons, D.R., Peakall, J., Paterson, D. M., Schindler, R.J., Ye, L., Lichtman, I.D., Bass, S.J., Davies, A.G., Manning, A.J., Thorne, P.D., 2015. The pervasive role of biological cohesion in bedform development. Nat. Commun. 6, 6257.
Meyers, P.A., 1994. Preservation of elemental and isotopic source identification of sedimentary organic matter. Chem. Geol. 114 (3), 289–302.
Montecillo, J.A.V., 2024. Comparative genomics of the genus *Halioglobus* reveals the genetic basis for the reclassification of *Halioglobus pacificus* as *Parahalioglobus pacificus* gen. Nov. comb. nov. Int. Microbiol. 27 (6), 1831–1838.
Mußmann, M., Pjevac, P., Krüger, K., Dyksma, S., 2017. Genomic repertoire of the *Woeseiaceae*/JTB255, cosmopolitan and abundant core members of microbial communities in marine sediments. ISME J. 11 (5), 1276–1281.
Nagler, M., Insam, H., Pietramellara, G., Ascher-Jenull, J., 2018. Extracellular DNA in natural environments: features, relevance and applications. Appl. Microbiol. Biotechnol. 102 (15), 6343–6356.
Nobu, M.K., Narihiro, T., Kuroda, K., Mei, R., Liu, W.T., 2016. Chasing the elusive Euryarchaeota class WSA2: genomes reveal a uniquely fastidious methyl-reducing methanogen. ISME J. 10 (10), 2478–2487.
Norbisrath, M., Pätsch, J., Dähnke, K., Sanders, T., Schulz, G., van Beusekom, J.E.E., Thomas, H., 2022. Metabolic alkalinity release from large port facilities (Hamburg, Germany) and impact on coastal carbon storage. Biogeosciences 19 (22), 5151–5165.
Pérez-Rodríguez, I., Choi, J.K., Abuyen, K., Tyler, M., Ronkowski, C., Romero, E., Trujillo, A., Tremblay, J., Viney, I., Savalia, P., Amend, J.P., 2021. *Geothermobacter hydrogeniphilus* sp. nov., a mesophilic, iron(III)-reducing bacterium from seafloor/subseafloor environments in the Pacific Ocean, and emended description of the genus *Geothermobacter*. Int. J. Syst. Evol. Microbiol. 71 (4).
Price, M.N., Dehal, P.S., Arkin, A.P., 2010. FastTree 2 - approximately maximum-likelihood trees for large alignments. PloS One 5 (3), e9490.
Quast, C., Pruesse, E., Yilmaz, P., Gerken, J., Schweer, T., Yarza, P., Peplies, J., Glöckner, F.O., 2013. The SILVA ribosomal RNA gene database project: improved data processing and web-based tools. Nucleic Acids Res. 41 (Database issue), D590–D596.
Reese, A., Zimmermann, T., Profrock, D., Irrgeher, J., 2019. Extreme spatial variation of Sr, Nd and Pb isotopic signatures and 48 element mass fractions in surface sediment of the Elbe River estuary - suitable tracers for processes in dynamic environments? Sci. Total Environ. 668, 512–523.
Sander, R., 2015. Compilation of Henry's law constants (version 4.0) for water as solvent. Atmos. Chem. Phys. 15 (8), 4399–4981.
Schoer, J.H., 1990. Determination of the origin of suspended matter and sediments in the Elbe estuary using natural tracers. Estuaries 13 (2), 161–172.
Schöl, A., Hein, B., Wyrwa, J., Kirchesch, V., 2014. Modelling water quality in the Elbe and its estuary – large scale and long term applications with focus on the oxygen budget of the estuary. Die Küste 81, 203–232.
Shakeel, A., Chassagne, C., Bornholdt, J., Ohle, N., Kirichek, A., 2022. From fundamentals to implementation of yield stress for nautical bottom: case study of the port of Hamburg. Ocean Eng. 266, 112772.
Silva, S.G., Nabhan Homsi, M., Keller-Costa, T., Rocha, U., Costa, R., 2023. Natural product biosynthetic potential reflects macroevolutionary diversification within a widely distributed bacterial taxon. mSystems 8 (6), e0064323.
Spieckermann, M., Gröngröft, A., Karrasch, M., Neumann, A., Eschenbach, A., 2022. Oxygen consumption of resuspended sediments of the upper Elbe estuary: process identification and prognosis. Aquat. Geochem. 28 (1), 1–25.
Straathof, A.L., Chincarini, R., Comans, R.N.J., Hoffland, E., 2014. Dynamics of soil dissolved organic carbon pools reveal both hydrophobic and hydrophilic compounds sustain microbial respiration. Soil Biol. Biochem. 79, 109–116.
Tolar, B.B., Mosier, A.C., Lund, M.B., and Francis, C.A. "Nitrosarchaeum" in Bergey's Manual of Systematics of Archaea and Bacteria, 1–9.
Van Zomeren, A., Comans, R.N., 2007. Measurement of humic and fulvic acid concentrations and dissolution properties by a rapid batch procedure. Environ. Sci. Technol. 41 (19), 6755–6761.
Vicena, J., Ardestani, M.M., Baldrian, P., Frouz, J., 2022. The effect of microbial diversity and biomass on microbial respiration in two soils along the soil chronosequence. Microorganisms 10 (10).
Wakeham, S.G., Lee, C., Hedges, J.I., Hernes, P.J., Peterson, M.L., 1997. Molecular indicators of diagenetic status in marine organic matter. Geochim. Cosmochim. Acta 61 (24), 5363–5369.
Wang, L., Wang, Y., Li, Y., Wang, L., Zhu, J., Zhang, W., Zhang, H., Niu, L., Wu, J., 2022. Effect of water chemistry on nitrogen transformation, dissolved organic matter composition and microbial community structure in hyporheic zone sediment columns. Environ. Res. 215 (Pt 1), 114246.
Wingender, J., Strathmann, M., Rode, A., Leis, A., Flemming, H.C., 2001. Isolation and biochemical characterization of extracellular polymeric substances from *Pseudomonas aeruginosa*. Methods Enzymol. 336, 302–314.
Wurpts, R., Torn, P., 2005. 15 years experience with fluid mud: definition of the nautical bottom with rheological parameters. Terra et Aqua 99, 22–32.
Zander, F., 2022. Turnover of Suspended and Settled Organic Matter in Ports and Waterways. Doctoral thesis. Delft University of Technology.
Zander, F., Groengroeft, A., Eschenbach, A., Heimovaara, T.J., Gebert, J., 2022. Organic matter pools in sediments of the tidal Elbe river. Limnologica 96.
Zander, F., Comans, R.N.J., Gebert, J., 2023. Linking patterns of physical and chemical organic matter fractions to its lability in sediments of the tidal Elbe river. Appl. Geochem. 156.